Engineering Development Studies for Molten-Salt Breeder Reactor Processing No. 18

J. R. Hightower, Jr.

OAK RIDGE NATIONAL LABORATORY

ORNL-TM-4698
UC-76 — Molten Salt Reactor Technology

Contract No. W-7405-eng-26

CHEMICAL TECHNOLOGY DIVISION

ENGINEERING DEVELOPMENT STUDIES FOR MOLTEN-SALT
BREEDER REACTOR PROCESSING NO. 18

J. R. Hightower, Jr.
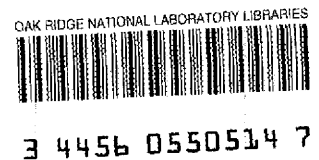
MARCH 1975

Reports previously issued in this series are as follows:

ORNL-TM-3053	Period ending December 1968
ORNL-TM-3137	Period ending March 1969
ORNL-TM-3138	Period ending June 1969
ORNL-TM-3139	Period ending September 1969
ORNL-TM-3140	Period ending December 1969
ORNL-TM-3141	Period ending March 1970
ORNL-TM-3257	Period ending June 1970
ORNL-TM-3258	Period ending September 1970
ORNL-TM-3259	Period ending December 1970
ORNL-TM-3352	Period ending March 1971

iii

CONTENTS

SUMMARIES

SALT-METAL CONTACTOR DEVELOPMENT

A water-mercury system was used to study the effect of geometric variations on mass transfer rates in rectangular contactors similar to those proposed for the MSBR fuel reprocessing scheme. Since mass transfer rates were not accurately predicted by the Lewis correlation, other correlations were investigated. The following correlation was found to fit the experimental results:

$$\frac{60\, k_1 L_1}{\nu_1} = 0.2058\ (Re_1)\left(\frac{\eta_2}{\eta_1}\right)^{1.4}\left(0.6 + \frac{\eta_2}{\eta_1}\right)^{-2.4} (Sc_1)^{-1/6}\left(\frac{\rho_2}{\rho_1}\right)^{0.27}\left(\frac{L}{H}\right)^{0.45}.$$

Mass transfer rates are being measured in a fluoride salt--bismuth contactor. A 6-in.-diam mild steel contactor has been installed in the flow-through reductive extraction facility for this purpose. Experimental results from these runs indicate that the mass transfer rates in the salt-bismuth system fall between the Lewis correlation and the modified correlation given above.

DEVELOPMENT OF THE METAL TRANSFER PROCESS: CONTINUATION OF ENGINEERING-SCALE EXPERIMENTS

Four engineering-scale experiments (MTE-1, -2, -2B, and -3) to study the steps in the metal transfer process were completed prior to the termination of the Molten-Salt Reactor Program early in 1973. The last experiment, MTE-3, used salt and bismuth flow rates that were 1% of the estimated flow rates required for processing a 1000-MW(e) reactor. We plan to continue these studies in a new experiment, designated as MTE-3B (identical to MTE-3).

The carbon steel vessels used in experiment MTE-3 are being replaced with new vessels. Fresh carrier salt, bismuth, and lithium chloride will be used.

Results of measurements of the mass transfer coefficients for radium, europium, lanthanum, and neodymium, obtained during operation of experiment MTE-3, indicated that many of the coefficients were lower than predicted by literature correlations. The reason for this is presently not known; consequently, additional studies are required in order to obtain data necessary for determining the size and type of equipment required for removal of the rare-earth fission products from molten-salt reactor fuel.

Examination of the MTE-3 carbon steel vessels indicated that no serious corrosion had occurred on the inside surfaces of the vessels exposed to salt and bismuth during 1 year of operation at 650°C (although the oxidation-resistant coating on the outside surface of the vessel failed to completely protect the carbon steel). Photomicrographs of the bismuth phases indicate that the surfaces in contact with the salts are enriched in thorium and iron.

CONTINUOUS FLUORINATOR DEVELOPMENT

Autoresistance heating tests have been continued in the fluorinator mock-up using $LiF-BeF_2-ThF_4$ (72-16-12 mole %) salt. The equipment was returned to operating condition, and five experiments were run. Although correct steady-state operation was not achieved, the results were encouraging.

A two-dimensional electrical analog was constructed to study current flow through the electrode sidearm and other critical areas of the test vessel. The model used constant-resistance paper cut in the shape of the sidearm. An electric field was produced between isopotential lines of conductive silver paint connected electrically to a constant-voltage source. The resulting flux lines were measured using a high-impedance voltmeter. These studies indicate that no regions of abnormally high current density existed in the first nine runs with the present autoresistance heating equipment. Localized heating had previously been the suspected cause for the failure to achieve proper operation of this equipment.

1. INTRODUCTION

A molten-salt breeder reactor (MSBR) will be fueled with a molten fluoride mixture that will circulate through the blanket and core regions of the reactor and through the primary heat exchangers. We are developing processing methods for use in a close-coupled facility for removing fission products, corrosion products, and fissile materials from the molten fluoride mixture.

In January 1973, the Molten Salt Reactor (MSR) Program was interrupted for about a year. The program was reinstated at ORNL again in January 1974, and the study of several operations associated with MSBR processing was resumed. The remaining parts of this report discuss:

(1) development of mechanically-agitated salt-metal contactors,

(2) examination of the vessels in which metal transfer experiment MTE-3 was carried out, and

(3) experiments of autoresistance heating of molten salts conducted in a mock-up of a frozen wall fluorinator.

This work was carried out in the Chemical Technology Division during the period January through June 1974.

2. SALT-METAL CONTACTOR DEVELOPMENT

J. A. Klein

A critical step in the proposed MSBR processing scheme is the extraction of rare earths from the fluoride fuel carrier salt to an intermediate bismuth stream. One possible approach would be to use a mechanically-agitated nondispersing contactor in which bismuth and fluoride salt phases are agitated in order to facilitate the mass transfer of rare earths across the salt-bismuth interface.

During the period covered by this report we have correlated mass transfer coefficients which were measured in a water-mercury system with those which were collected from the open literature for aqueous-organic systems. We have completed four experiments in which mass transfer

coefficients in a fluoride salt-bismuth system were measured. This work
is discussed in the following sections.

2.1 Background

Lewis[1] investigated mass transfer rates in mechanically-agitated
nondispersing contactors, all of the same size, using several aqueous-
organic systems. He fitted his results with the following empirical
equation:

$$\frac{60 \, k_1 L}{\nu_1} = 6.76 + 10^{-6} \, (L) \left(Re_1 + Re_2 \frac{\eta_2}{\eta_1} \right)^{1.65} + 1 \, , \tag{1}$$

where

Re = Reynolds number = $\dfrac{NL^2 \rho}{\eta}$,

N = stirrer speed = rps,

L = stirrer length = cm,

k = mass transfer coefficient, cm/sec,

ρ = density = g/cm^3,

η = viscosity = g/cm·sec,

ν = kinematic viscosity = η/ρ = cm^2/sec, and

$1,2$ = phase being considered.

For the case in which $N_1 = N_2$ and $L_1 = L_2$, the above equation can be
reduced to the form

$$\frac{60 \, k_1 L}{\nu_1} = 6.76 \times 10^{-6} \, (L) \left[Re_1 \left(1 + \frac{\rho_2}{\rho_1} \right) \right]^{1.65} + L \, . \tag{2}$$

For Lewis' work, where the densities of the various phases varied from
0.8 to 1.2 g/cm^3 but the stirrer length was kept constant, this correla-
tion effectively uses only the Reynolds number of the phase being con-
sidered.

McManamey[2] correlated his own data with Lewis's results by the following expression, which is similar to that used by Lewis but includes the Schmidt number:

$$\frac{60\ k_1 L_1}{\eta_1} = 0.102\ (L)(Re_1)^{0.9}\left(1 + \frac{\eta_2}{\eta_1}\frac{Re_2}{Re_1}\right)(Sc_1)^{-0.37}\ , \tag{3}$$

where

Sc = Schmidt number = $\eta/\rho D$, and

D = diffusion coefficient = cm^2/sec.

Note that the dependence on the Schmidt number is fairly weak. This equation can be reduced to:

$$\frac{60\ k_1 L}{\nu_1} = 0.102\ (L)(Re_1)^{0.9}\left(1 + \frac{\rho_1}{\rho_2}\right)(Sc_1)^{-0.37}\ . \tag{4}$$

Again, the Reynolds number of the phase being considered is the dominant factor, although it is raised to a different power from that used by Lewis (i.e., 0.9 rather than 1.65).

Mayers[3] developed a slightly more involved correlation of the following form:

$$\frac{60\ k_1 L_1}{\nu_1} = 0.1896\ (Re_1\ Re_2)^{1/2}\left(\frac{\eta_2}{\eta_1}\right)^{1.9}\left(0.6 + \frac{\eta_2}{\eta_1}\right)^{-2.4}(Sc_1)^{-1/6}\ . \tag{5}$$

This equation reduces to:

$$\frac{60\ k_1 L}{\nu_1} = 0.1896\ (Re_1)\left(\frac{\eta_2}{\eta_1}\right)^{1.4}\left(0.6 + \frac{\eta_2}{\eta_1}\right)^{-2.4}(Sc_1)^{-1/6}\left(\frac{\rho_2}{\rho_1}\right)^{0.5}\ . \tag{6}$$

This correlation indicates that the viscosity and density of each phase affect the mass transfer coefficient. This correlation is based on data covering a limited range of densities (0.8 to 1.2 g/cm^{3}).

All of the above equations correlate the large amount of aqueous-organic data very well; the Mayers and McManamey correlations provide a slightly better fit than the Lewis correlation. However, in all cases, N, n_1, and n_2 were the only parameters varied to any significant extent. The other variables were either held constant or were varied over very small ranges.

2.2 Experimental Studies Using Water-Mercury Systems

Previous reports[4,5] have shown that a water-mercury contactor using the reaction

$$Pb^{2+} [H_2O] + Zn [Hg] \rightarrow Zn [Hg] + Zn^{2+} [H_2O]$$
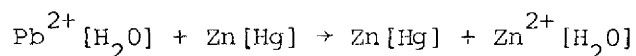
is suitable for studying mass transfer rates in this system. These studies have indicated that, although results were generally similar to the predictions of the Lewis correlation, significant deviations from the correlation do exist. In order to reconcile these discrepancies, we have studied the effect of geometric variations on mass transfer rates in rectangular contactors similar to those proposed for the MSBR fuel reprocessing scheme.

2.2.1 Experimental procedures

Three rectangular contactors were fabricated in the following sizes: 5-1/4 in. x 7 in., 7-3/4 in. x 10-1/2 in., and 11-5/8 in. x 12-1/2 in. The two smaller vessels were constructed of Plexiglas, while the larger was constructed of stainless steel.

Agitator blades having diameters of 3, 5, and 7 in. were fabricated. One set of blades had a constant height of 3/4 in.; another set had a constant blade diameter/blade height ratio of 4.0. All of the blades were four-vaned straight paddles.

Each contactor was used to make a large number of experimental runs in which the phase volume, blade size, and agitation rates were varied. Agitation rates were limited to values below the point at which dispersion

of the phases became apparent. The paddles used in the two phases were identical in size.

Details of sampling and analysis of data are included in a previous report.[4]

2.2.2 Results

Results obtained using the 7-3/4- by 10-1/2-in. contactor and a 5000-cm volume for each phase are compared with the three correlations in Figs. 1-3. Similar results were obtained for other contactor sizes. Table 1 gives the data for the water-mercury system. Phase 1 is mercury; phase 2 is water.

Experimental mass transfer coefficients ranged from 5 to 30% of the values predicted by the Lewis correlation. The slope of the data deviated significantly from that of the Lewis correlation; it agreed very closely with the slope of the McManamey correlation, although experimental values were only 15 to 30% of predicted values. Thus it appears that the McManamey correlation is only slightly better than the Lewis correlation. The slope of the Mayers correlation also matches that of the data very well but underpredicts experimental results by 40 to 50%.

The results shown in Figs. 1 and 2, as well as the remainder of the data, indicate that the mass transfer coefficient is proportional to the stirrer length, L, raised to a power different from that associated with the Reynolds number. The exponent of L is 1 in the Mayers correlation rather than approximately 2 as in the other correlations. This change improves the correlation; however, it also seems to overcompensate to some extent.

Using the Mayers correlation as the best of the existing correlations, we added two additional terms to include the effect of the density ratio of the two phases (ρ_1/ρ_2) and a dimension ratio (L/H), where H is the height of an individual phase. The tank size or phase volume was shown to be unimportant except in the manner in which it affects H.
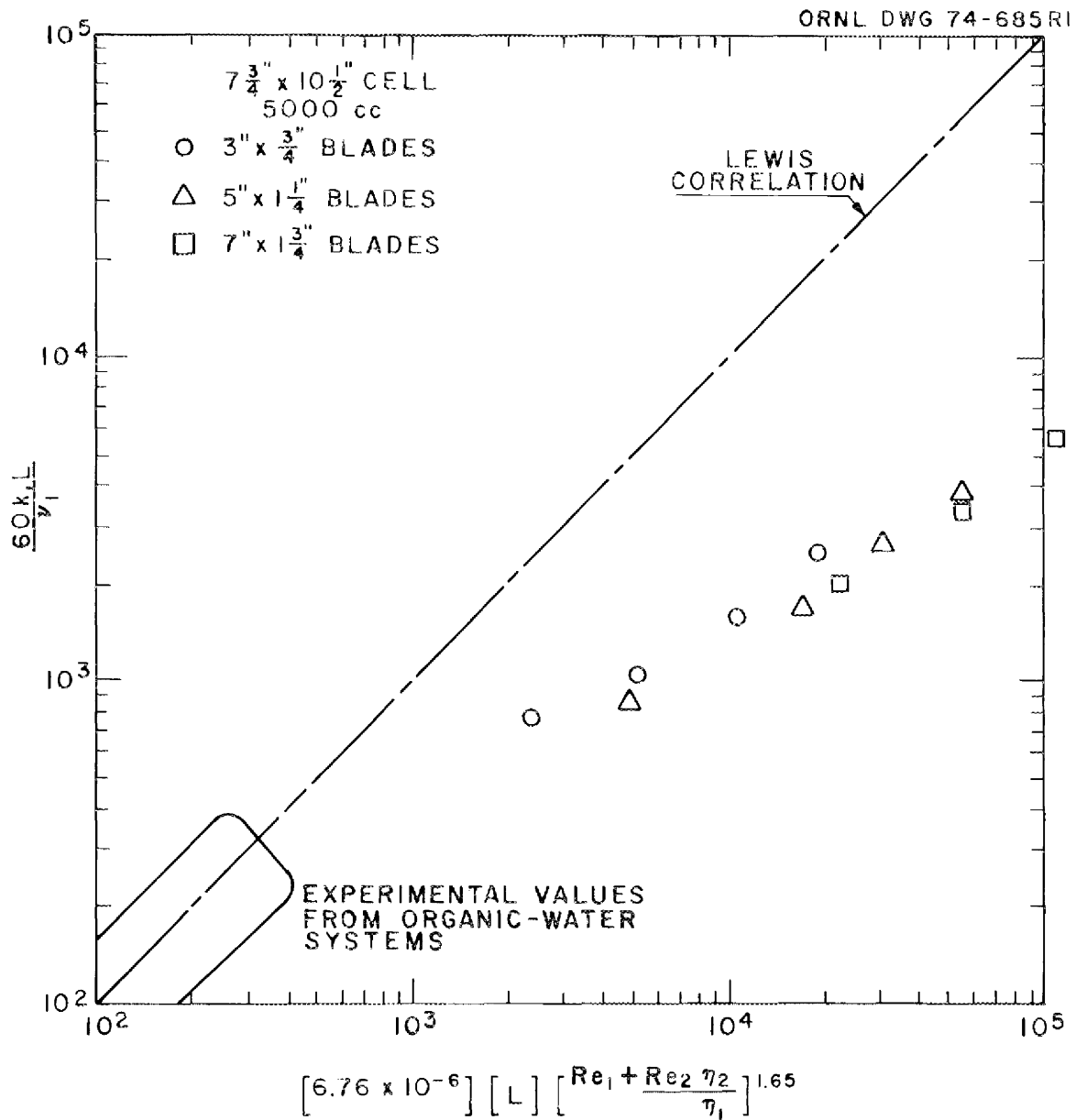
Fig. 1. Selected experimental results as compared with the Lewis correlation for the water-mercury system.
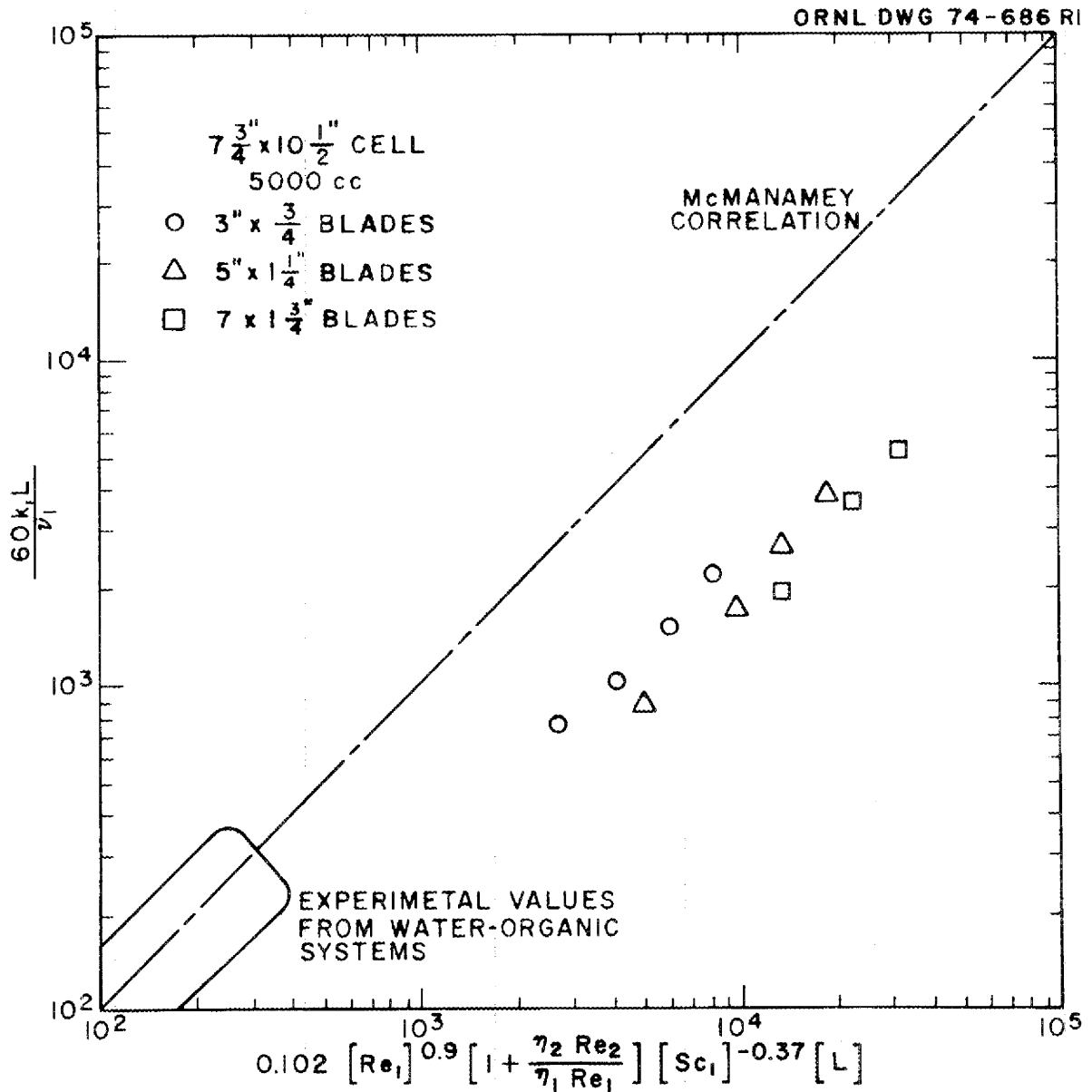
Fig. 2. Selected water-mercury experimental results as compared with the McManamey correlation.
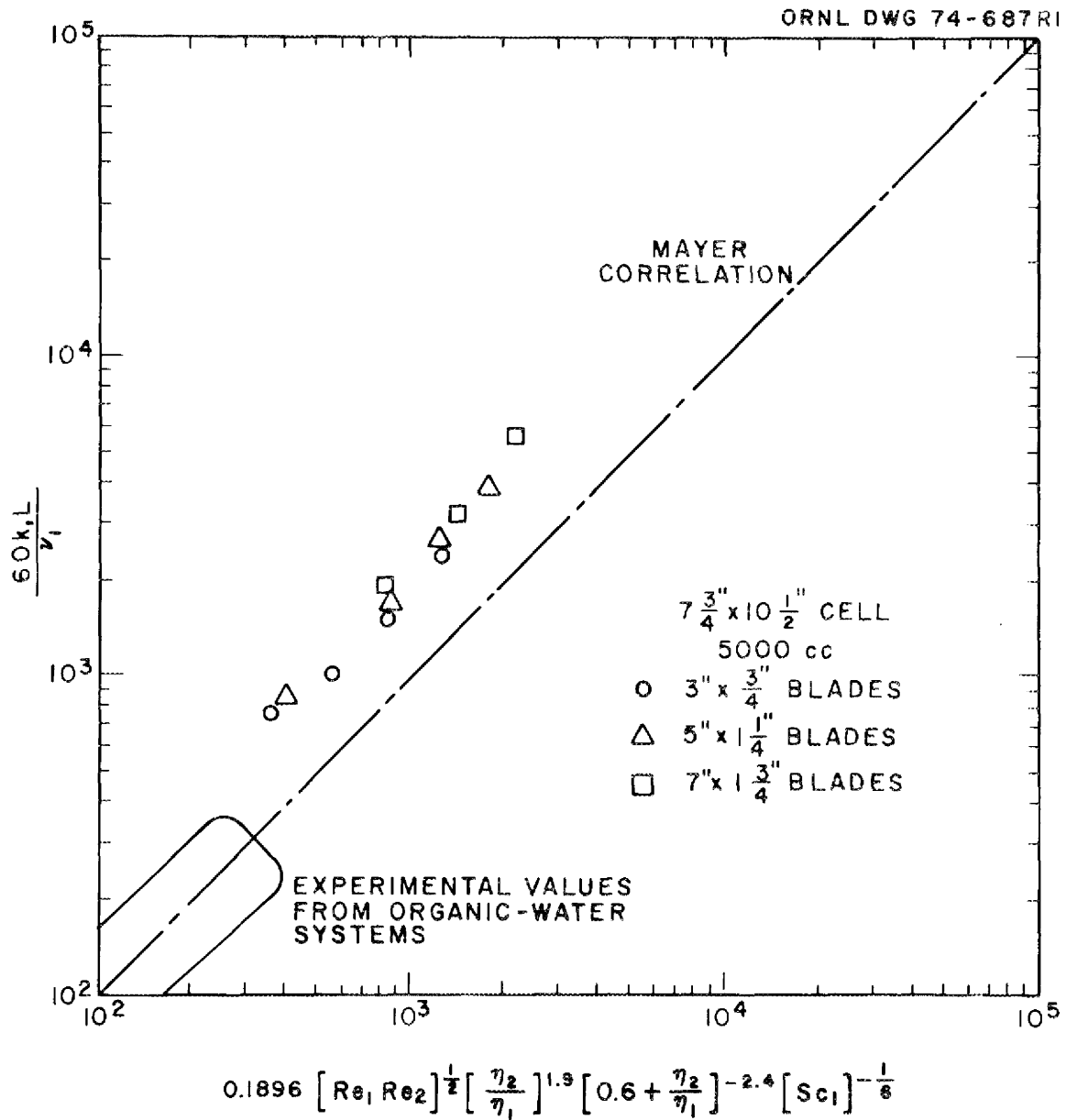
8

Fig. 3. Selected experimental results as compared with the Mayer correlation for the water-mercury system.

Table 1. Experimental and predicted mass transfer rates for the water-mercury system

Run No.	Contactor size (cm)	(L) Blade size (diam x height)	Phase volume (cc)	(H) Phase depth (cm)	(N) Stirrer speed (rpm)	$\frac{60\,k_1L}{v_1}$ Predicted value[a]	Experimental value
1	13.3 x 17.8	7.62 x 1.90	1,200	5.2	55	917	836
2			1,200	5.2	72	1200	577
3			1,200	5.2	98	1634	1457
5			1,200	5.2	136	2267	3078
10			1,800	7.8	53	736	689
11			1,800	7.8	70	972	645
12			1,800	7.8	99	1375	1313
13			1,800	7.8	150	2083	2710
14			1,800	7.8	180	2500	3956
20			2,600	11.0	51	607	428
21			2,600	11.0	70	833	517
22			2,600	11.0	126	1499	2025
23			2,600	11.0	183	2177	3034
24			2,600	11.2	205	2420	3711
35		12.70 x 3.175	1,200	5.3	29	1676	1849
36			1,200	5.0	49	2906	3318
37			1,800	7.5	29	1433	1609
38			1,800	7.5	50	2471	3811
39			2,600	11.0	29	1206	1017
40			2,600	11.0	51	2121	3377
41			2,600	11.0	81	3369	6294
42	19.7 x 26.7	7.62 x 1.90	3,000	5.5	51	829	476
43			3,000	5.5	77	1252	1064
44			3,000	5.5	123	1999	1919
45			5,000	9.5	50	635	756
46			5,000	9.5	80	1017	1024
47			5,000	9.5	120	1525	1548
48			5,000	9.5	181	2300	2507
49			7,000	13.5	53	575	765
50			7,000	13.2	78	855	1045
51			7,000	13.5	127	1378	956
52			7,000	13.2	185	2028	1839
53			9,000	17.1	51	498	421
54			9,000	17.0	82	802	843
55	19.7 x 26.7	7.62 x 1.90	9,000	17.0	125	1223	1022
56			9,000	17.0	150	1467	1234
70		12.70 x 3.175	3,000	5.5	21	1193	959
71			3,000	6.0	41	2240	1840
72			3,000	6.0	59	3223	2521
73			3,000	6.0	79	4316	3485
74			5,000	9.5	20	889	884
75			5,000	9.5	44	1955	1681
76			5,000	9.5	61	2710	2769
77			5,000	9.5	75	3332	4329
78			7,000	13.5	21	797	869
79			7,000	13.5	40	1517	1144
80			7,000	13.5	60	2276	2046
81			7,000	13.5	80	3035	3133
82			7,000	13.5	89	3376	3534
83			9,000	17.0	20	684	776
84			9,000	17.0	41	1402	1372
85			9,000	17.2	60	2041	1853
86			9,000	17.2	80	2721	2690
100		17.78 x 4.44	3,000	5.8	21	2657	2640
101			3,000	5.8	41	5185	5094
102			3,000	5.8	48	6073	7350
103			5,000	9.5	21	2128	2169
104			5,000	9.5	35	3546	4223
105			5,000	9.5	50	5066	6104
106			7,000	13.5	20	1730	1440
107			7,000	13.5	35	3028	3392
108			7,000	13.5	52	4498	6091
109			9,000	17.2	22	1707	2118
110			9,000	17.5	39	3002	3314
111			9,000	17.5	47	3617	4566
130	29.5 x 31.8	12.70 x 3.17	25,000	26.8	32	892	1167
131			25,000	26.9	51	1418	1435
132			25,000	26.2	80	2252	1881

$$^a 0.2058 \, (Re_1) \left(\frac{\eta_2}{\eta_1}\right)^{1.4} \left(0.6 + \frac{\eta_2}{\eta_1}\right)^{-2.4} (Sc_1)^{-1/6} \left(\frac{\rho_2}{\rho_1}\right)^{0.27} \left(\frac{L}{H}\right)^{0.45}$$

A linear regression which was performed on all the new experimental data to determine the exponents on (ρ_1/ρ_2) and (L/H) yielded the following:

$$\frac{60 \, k_1 L_1}{\nu_1} = 0.2058 \, [Re_1 Re_2]^{1/2} \left[\frac{\eta_2}{\eta_1}\right]^{1.9} \left[0.6 + \frac{\eta_2}{\eta_1}\right]^{-2.4} [Sc_1]^{-1/6} \left[\frac{\rho_1}{\rho_2}\right]^{0.23} \left[\frac{L_1}{H}\right]^{0.45} .$$

(7)

For the case in which the blades in each phase have identical dimensions and stirring rates, this reduces to:

$$\frac{60 \, k_1 L}{\nu_1} = 0.2058 \, [Re_1] \left[\frac{\eta_2}{\eta_1}\right]^{1.4} \left[0.6 + \frac{\eta_2}{\eta_1}\right]^{-2.4} [Sc_1]^{-1/6} \left[\frac{\rho_2}{\rho_1}\right]^{0.27} \left[\frac{L}{H}\right]^{0.45} . \quad (8)$$

The constant was determined using the aqueous-organic systems as well as the mercury-water system. Thus the new correlation predicts the aqueous-organic systems as accurately as the Mayer correlation.

The modified correlation fits the experimental water-mercury data with a standard deviation at 25%, as shown in Fig. 4.

2.3 Comparison of Correlations with MTE-3 Data

A comparison of the mass transfer coefficients reported[6] from the experiment MTE-3 with both the Lewis and modified correlations was made in order to test the fit of the correlations with an actual salt-bismuth system. Results of the comparison are shown in Table 2. The data indicate that, while the Lewis correlation vastly overpredicts the mass transfer coefficients, the modified correlation usually underpredicts them —

ORNL DWG 74-683RI

$5\frac{1}{4}$" x 7" CELL

O	1200 cc	3"x $\frac{3}{4}$" BLADES	
◐	1800 cc	"	
◑	2600 cc	"	
□	1200 cc	5"x $1\frac{1}{4}$" BLADES	
◪	1800 cc	"	
◩	2600 cc	"	

$11\frac{5}{8}$" x $12\frac{1}{2}$" CELL

+ 2500 cc 5"x $1\frac{1}{4}$" BLADES

$7\frac{3}{4}$" x $10\frac{1}{2}$" CELL

△	3000 cc	3"x $\frac{3}{4}$" BLADES	
◭	5000 cc	"	
▲	7000 cc	"	
▲	9000 cc	"	
▽	3000 cc	5"x $1\frac{1}{4}$" BLADES	
▼	5000 cc	"	
▼	7000 cc	"	
▼	9000 cc	"	
⬡	3000 cc	7"x $1\frac{3}{4}$" BLADES	
⬣	5000 cc	"	
⬣	7000 cc	"	
⬢	9000 cc	"	

+25%

-25%

$\dfrac{60 k_1 L}{\nu_1}$

10^4 10^3 10^2

10^2 10^3 10^4

$$0.2058 \left[Re_1 \, Re_2 \right]^{\frac{1}{2}} \left[\frac{\eta_2}{\eta_1} \right]^{1.9} \left[0.6 + \frac{\eta_2}{\eta_1} \right]^{-2.4} \left[Sc_1 \right]^{-\frac{1}{6}} \left[\frac{\rho_1}{\rho_2} \right]^{0.23} \left[\frac{L}{H} \right]^{0.45}$$
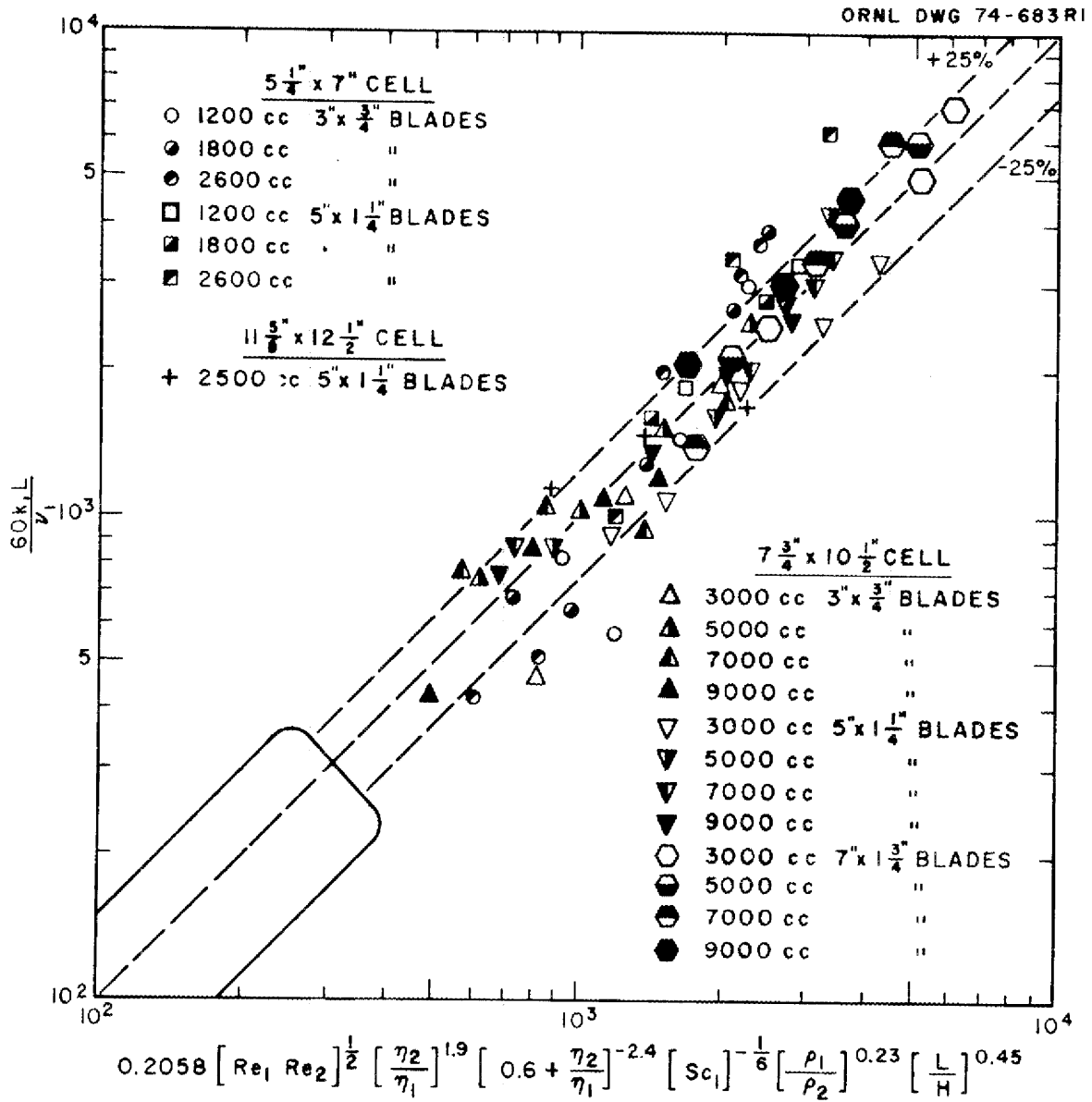
Fig. 4. Experimental water-mercury results as fit by the modified mass-transfer correlation.

Table 2. Mass transfer coefficients from MTE-3 as compared
with the Lewis and modified correlations

Material	Agitator speed (rpm)	K_1 (cm/sec)[a]			K_2 (cm/sec)[b]			K_3 (cm/sec)[c]		
		Measured value	Percent of Lewis	Percent of modified	Measured value	Percent of Lewis	Percent of modified	Measured value	Percent of Lewis	Percent of modified
Europium	100	1.0×10^{-4}	30	400	1.5×10^{-6}	10	71	1.1×10^{-3}	10	85
	200	3.0×10^{-4}	30	600	4.8×10^{-6}	10	112	3.3×10^{-3}	10	127
Lanthanum	100	6.0×10^{-5}	15	286	3.9×10^{-5}	0.5	3	6.2×10^{-3}	7	151
	150	1.4×10^{-4}	15	438	1.1×10^{-4}	0.5	6	1.2×10^{-2}	7	197
	200	2.0×10^{-4}	15	465	1.3×10^{-4}	0.5	5	2.0×10^{-2}	7	247
	200	2.0×10^{-4}	15	465	2.0×10^{-3}	10	77	2.0×10^{-2}	7	247
	300	2.6×10^{-4}	15	406	3.2×10^{-3}	10	82	2.0×10^{-2}	4	167
	300	2.6×10^{-4}	15	406	3.2×10^{-3}	10	82	2.0×10^{-2}	4	167
Neodymium	200	2.0×10^{-4}	15	339	6.5×10^{-3}	10	162	2.0×10^{-2}	7	247
	300	3.0×10^{-4}	15	341	1.1×10^{-2}	10	186	2.0×10^{-2}	4	167

[a]K_1 measured at fluoride salt--Bi-Th interface.

[b]K_2 measured at LiCl--Bi-Th interface.

[c]K_3 measured at LiCl--Li-Bi interface.

salt-bismuth flow-through facility. This experimental system (Fig. 5) allows (1) periodic cleaning of the feed salt and metal, (2) removal of surface contamination from the salt-metal interface, and (3) variation of the distribution ratio of the material of interest between the salt and the bismuth.

2.4.1 Experimental equipment

The new stirred-interface contactor makes use of the existing piping, equipment, and instrumentation present in the mild-steel reductive extraction system. The contactor, which is geometrically identical to that used with the water-mercury system, consists of a 6-in.-diam carbon-steel vessel containing four 1-in.-wide vertical baffles. The agitator consists of two 3-in.-diam stirrers with four noncanted blades. A 3/4-in. overflow at the interface allows for removal of interfacial films, as well as the salt and metal outflow. The system is operated in essentially the same manner as was employed with the packed column.[7-11] The salt and bismuth phases were equilibrated prior to an experiment. After the salt and metal phases had been transferred to the feed tanks, ^{97}Zr and ^{237}U tracers were added to the salt. With this technique the rates at which zirconium and uranium tracer transfer from the salt to the bismuth could be measured in a system that was otherwise at chemical equilibrium.

2.4.2 Mathematical analysis

For a flow-through, continuously stirred contactor at steady-state conditions, a mass balance on the salt phase yields:

$$F_1 C_1 = F_1 C_s + J , \qquad (9)$$

where

F_1 = flow rate of salt, cm^3/sec,

C_1 = tracer concentration in salt inflow, units/cm^3,

C_s = tracer concentration in salt outflow, units/cm^3,

J = rate of transfer of tracer across the interface, units/sec.
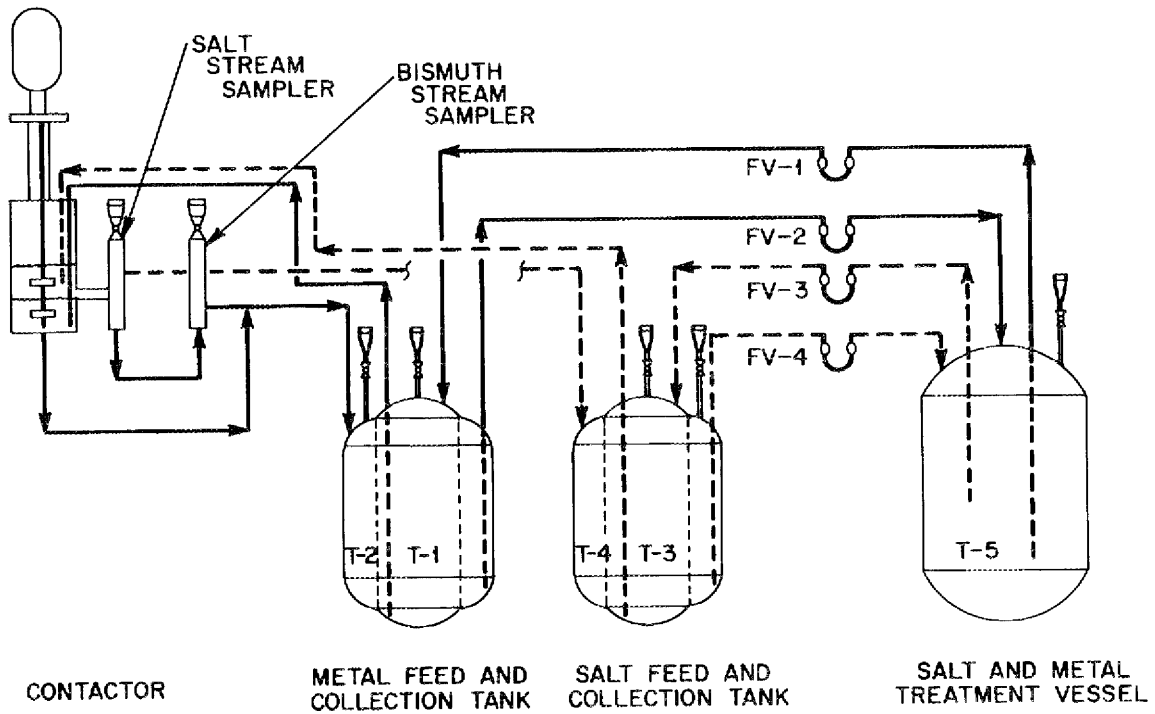
ORNL DWG 74-694R1

Fig. 5. Salt-metal contactor as installed in the mild-steel reductive extraction facility.

Expressing the rate of transfer across the interface as the product of an overall mass transfer coefficient and a driving force times the area available for mass transfer yields:[12]

$$J = K_s [C_s - C_m/D] A , \tag{10}$$

where

$$1/K_s = 1/k_s + 1/Dk_m , \tag{11}$$

and

K_s = overall mass transfer coefficient based on salt phase, cm/sec,

k_s = individual mass transfer coefficient in salt phase, cm/sec,

k_m = individual mass transfer coefficient phase in metal, cm/sec,

D = distribution coefficient = ratio of concentration in metal phase to concentration in salt phase at equilibrium, $\dfrac{\text{moles/cm}^3}{\text{moles/cm}^3}$,

C_m = tracer concentration in metal outflow, units/cm^3, and

A = interfacial area, cm^2.

Taking an overall mass balance gives:

$$C_1 F_1 + C_2 F_2 = C_s F_1 + C_m F_2 , \tag{12}$$

where

C_2 = tracer concentration in metal inflow, units/cm^3, and

F_2 = flow rate of metal, cm^3/sec.

If $C_2 = 0$, Eq. (12) can be rearranged to give the four following relations:

$$C_1 F_1 = C_s F_1 + C_m F_2 , \tag{13}$$

$$C_1 = C_s + C_m\left(\frac{F_2}{F_1}\right) , \tag{14}$$

$$C_s = C_1 - C_m\left(\frac{F_2}{F_1}\right) , \text{ and} \tag{15}$$

$$C_m = C_1\frac{F_1}{F_2} - C_s\left(\frac{F_1}{F_2}\right) . \tag{16}$$

Combining Eqs. (9), (10), and (16) yields:

$$F_1C_1 = F_1C_s + K_sC_sA - \frac{K_sC_1A}{D}\left(\frac{F_1}{F_2}\right) + \frac{K_sC_sA}{D}\left(\frac{F_1}{F_2}\right) , \tag{17}$$

which can be rearranged to give:

$$C_s/C_1 = \frac{F_1 + \frac{K_sA}{D}(F_1/F_2)}{F_1 + K_sA + \frac{K_sA}{D}\left(\frac{F_1}{F_2}\right)} . \tag{18}$$

Combining Eqs. (9), (10), and (15) yields:

$$F_1C_1 = F_1C_1 - C_mF_2 + K_sC_1A - (K_sC_mA)\frac{F_2}{F_1} - \left(\frac{K_sC_mA}{D}\right) , \tag{19}$$

which is rearranged to give:

$$C_m/C_1 = \frac{K_sA}{F_2 + (K_sA)\frac{F_2}{F_1} + \left(\frac{K_sA}{D}\right)} . \tag{20}$$

Combining Eqs. (9), (10), and (14) yields:

$$F_1C_s + C_mF_2 = F_1C_s + K_sC_sA - \left(\frac{K_sC_mA}{D}\right) , \tag{21}$$

which is arranged to give:

$$C_m/C_s = \frac{K_s A}{F_2 + \left(\dfrac{K_s A}{D}\right)} \, . \tag{22}$$

Rearranging Eqs. (18), (20), and (22) gives three expressions for the overall mass transfer coefficient in terms of the measured quantities C_1, C_s, C_m, F_1, F_2, D, and A:

$$K_s = \frac{F_1 \left(1 - \dfrac{C_s}{C_1}\right)}{A\left(\dfrac{C_s}{C_1}\right) + \dfrac{A}{D}\left(\dfrac{C_s}{C_1}\right)\left(\dfrac{F_1}{F_2}\right) - \dfrac{A}{D}\left(\dfrac{F_1}{F_2}\right)} \, , \tag{23}$$

$$K_s = \frac{\left(\dfrac{C_m}{C_1}\right) F_2}{A - A\left(\dfrac{C_m}{C_1}\right)\left(\dfrac{F_2}{F_1}\right) - \left(\dfrac{C_m}{C_1}\right)\left(\dfrac{A}{D}\right)} \, , \text{ and} \tag{24}$$

$$K_s = \frac{\left(\dfrac{C_m}{C_s}\right) F_2}{A - \left(\dfrac{C_m}{C_s}\right)\left(\dfrac{A}{D}\right)} \, . \tag{25}$$

The above equations can then be used to calculate mass transfer coefficients from experimental results (i.e., the ratio of tracer concentrations in any two of the salt or bismuth flows).

Approximately 10-liter volumes of salt and bismuth were available, allowing flow rates up to 200 cc/min. Experimental values of D, the distribution coefficient for the material of interest, will vary somewhat; however, if D is made large enough, Eqs. (23), (24), and (25) reduce to:

$$K_s = \frac{F_1}{A}\left(\frac{1 - \left(\frac{C_s}{C_1}\right)}{\left(\frac{C_s}{C_1}\right)}\right) , \tag{26}$$

$$K_s = \frac{F_2}{A}\left(\frac{\left(\frac{C_m}{C_1}\right)}{1 - \left(\frac{F_2}{F_1}\right)\left(\frac{C_m}{C_1}\right)}\right) , \text{ and} \tag{27}$$

$$K_s = \frac{F_2}{A}\frac{C_m}{C_s} . \tag{28}$$

Uncertainties in the distribution coefficient do not affect the accuracy of the overall mass transfer coefficient. However, when D is very large, the overall mass transfer coefficient is essentially the individual salt-phase coefficient since resistance to mass transfer in the metal phase is negligible in comparison. This is seen by allowing D to assume large values in Eq. (11).

2.4.3 Experimental results

Four runs have been completed to date. All runs were performed in a similar manner except as discussed below.

While the fluoride salt and bismuth are in contact in T5, the treatment vessel, a sufficient quantity of beryllium is electrolytically added to the salt to give any desired uranium distribution coefficient (D_u). Since it is impossible to completely exclude oxidants, beryllium needs to be added periodically in order to maintain a relatively high distribution coefficient. Periodic transfers of salt and bismuth throughout the system are also performed to maintain the system at equilibrium.

Prior to a run, the salt and bismuth phases were separated by pressurizing T5 and transferring salt to T3 and bismuth to T1. Approximately 7 mCi of ^{97}Zr-^{97}Nb and 50 to 100 mCi of ^{237}U$_3$O$_8$ were then allowed to dissolve in the salt phase for about 2 hr. Activities of the ^{95}Zr and ^{236}U, which were also present, were negligible.

Salt and bismuth streams were passed through the contactor vessel by controlled pressurization of both T1 and T3. The contactor was maintained at approximately 590°C for each run. Both phases exit through a common overflow line, separate, and return to tanks T2 and T4. Periodic sampling of both exit streams was accomplished by means of flowing stream samplers installed in the exit lines from the contactor.

Samples taken were first counted for ^{237}U and ^{97}Zr, then pulverized, dissolved, and counted again for ^{237}U (at this point, ^{97}Zr had decayed to a very low level). Counting twice was done in order to correct for the self-absorption in the solid salt or bismuth samples of the 207.95-keV β^- from ^{237}U. No similar correction for the self-absorption of the ^{97}Zr-^{97}Nb (743.37 keV and 658.18 keV β^-, respectively) activity could be done because of the shorter half-life. A complete wet analysis was also run on each sample. Mass transfer rates could then be calculated from the ratios of tracer concentrations as discussed previously.

Run TSMC-1 was mainly a preliminary experiment designed to test the procedure. In this run, the salt and bismuth flows were approximately 200 cc/min and the stirrer rate was 123 rpm. Unfortunately, the distribution coefficient was too low to effect any significant mass transfer; thus mass transfer rates could not be accurately determined.

Run TSMC-2 was performed without difficulty. The salt and bismuth flow rates were 228 and 197 cc/min, respectively. The distribution coefficient for this run was determined to be approximately 1.5, which was lower than desired but high enough to give meaningful results.

A bismuth line failure occurred immediately preceding run TSMC-3. During the resulting delay for repairs, the ^{97}Zr decayed and only the ^{237}U tracer could be used. The remainder of the run went smoothly. The salt and bismuth flow rates were 166 and 173 cc/min, respectively; the stirrer rate was 162 rpm. A high D_u (> 40) was maintained for this run.

In run TSMC-4, flow rates of 170 and 144 cc/min were set for the salt and bismuth flows; a stirrer rate of 205 rpm was maintained. Both distribution coefficients as determined from samples taken before, after, and during the run were greater than 200. [This value is sufficiently large that Eqs. (26-28) are valid.] Large distribution coefficients cannot be determined precisely due to the inability to determine very small amounts of uranium in the salt phase. No significant problems were encountered during this run.

Results for these four runs are shown in Table 3. As noted previously, results from run TSMC-1 are not meaningful. The three equations for determining the mass transfer rates [Eqs. (26), (27), and (28)] were used to calculate values for the mass transfer coefficient.

2.5 Contactor Area Required for MSBR Processing Plant

An estimate of the area required for a one-stage contactor for removing rare earths from the fuel salt can be made by using the mass transfer coefficients measured in the salt-bismuth flow-through facility.

The flowsheet assumes a total reactor fuel salt volume of 47,500 liters, with a salt flow of 55 cc/sec; this would give a 10-day removal time for the salt. Of the rare earths, cerium has the shortest removal time (16.6 days). Therefore, approximately a 60% efficiency is needed for the proposed stirred interface contactor.

From Eq. (18),

$$C_s/C_1 = \frac{F_1 + \dfrac{K_s A}{D}(F_1/F_2)}{F_1 + K_s A + \dfrac{K_s A}{D}(F_1/F_2)} = 0.60 \tag{29}$$

if D is made large and the following reference values are used:

F_2 = 780 cc/sec = bismuth flow rate,

F_1 = 55 cc/sec = salt flow rate, and

area = $36.7/K_s$.

Substituting values of mass transfer coefficient from Table 3 into Eq. (29) gives the following results:

Table 3. Experimental results from the salt-metal contactor

Run	Salt flow (cc/min)	Bismuth flow (cc/min)	Stirrer rate (rpm)	D_u	Fraction tracer transferred[a]	K_s (cm/sec)[b] Experimental K_{s_1}	K_{s_2}	K_{s_3}	Correlations Lewis	Modified
TSMC-1	212	193	123	∿0.02	∿0	∿0	0.0014	0.0012	0.00030	0.000043
TSMC-2	228	197	121	1.5	0.17	0.0043	0.0090	0.0070	0.020	0.0012
TSMC-3	166	173	162	>40	0.50	0.015	0.0099	0.012	0.032	0.0017
TSMC-4	170	144	205	>200	0.78	0.055	0.052	0.054	0.051	0.0021

[a]Fraction tracer transferred $= 1 - \dfrac{C_s}{C_l}$.

[b]$K_{s_1} = K_s = \dfrac{F_1}{A}\left(\dfrac{1 - \dfrac{C_s}{C_l}}{\dfrac{C_s}{C_l}}\right)$, $K_{s_2} = K_s = \dfrac{F_2}{A}\left(\dfrac{C_m/C_l}{1 - \left(\dfrac{F_2}{F_1}\right)\left(\dfrac{C_m}{C_l}\right)}\right)$, and $K_{s_3} = K_s = \dfrac{F_2}{A}\left(\dfrac{C_m}{C_s}\right)$.

if K_s = 0.0042 cm/sec = lowest experimental value,

A = 9 ft^2; and

if K_s = 0.054 cm/sec = highest experimental value,

A = 0.7 ft^2.

These values for the area of the proposed contactor would seem to be quite reasonable. However, the actual area which would be required for a contactor in a processing plant would be somewhat larger because the distribution coefficient in the contactor would not be as large as was assumed in the above calculation.

2.6 Conclusions

A new correlation has been developed to account for the effect of large density differences and variations in the stirrer length/phase depth ratio. The correlation given in Eq. (7) accurately predicts the experimental results for the water-mercury system as well as the results for the aqueous-organic systems reported in the literature. A flow-through, stirred-interface contactor was installed in the mild-steel reductive extraction facility. Mass transfer rates for a molten fluoride salt--bismuth system were measured using this contactor. These measured rates fell between the predictions made by the Lewis and modified correlations, except when high stirrer rates were used; in the latter cases, high mass transfer rates were obtained. If these values of mass transfer coefficient prevail, the required mass transfer area in an MSBR processing plant would not be unreasonably large.

3. DEVELOPMENT OF THE METAL TRANSFER PROCESS: CONTINUATION
OF ENGINEERING-SCALE EXPERIMENTS

H. C. Savage

The present processing flowsheet[13] uses the metal transfer process
for removing rare earths from molten-salt breeder reactor fuel salt. In
this process, fuel salt that is free of uranium and protactinium but con-
tains the rare earths is countercurrently contacted with bismuth containing
reductant to extract the rare earths into the bismuth. The bismuth stream,
which contains the rare earths and thorium, is then countercurrently con-
tacted with LiCl. Because of favorable distribution coefficients, signif-
icant fractions of the rare earths transfer to the LiCl along with a
negligible amount of thorium. The final steps of the process consist in
extracting the rare earths from the LiCl by contact with bismuth having
lithium concentrations of 5 and 50 at. %.

Four engineering-scale experiments (MTE-1, -2, -2B, -3) have been
carried out to study the steps in the metal transfer process and to obtain
information such as mass transfer rates of the rare earths between the
salt and bismuth phases necessary for determining the size and type of
equipment needed for the process. The results obtained in these experi-
ments were reported previously.[14-17] The selective removal of rare earths
(lanthanum and ^{147}Nd) from MSBR fuel carrier salt (72-16-12 mole % LiF-
BeF_2-ThF_4) and transfer to Li-Bi acceptor alloy were demonstrated in
experiments MTE-1, -2, and -2B. MTE-3 was a larger-scale experiment,
which included features such as mechanical agitation of the salt and
metal phases to improve mass transfer rates of the rare earths across the
three salt-metal interfaces. This experiment was designed to measure the
mass transfer rates across the three interfaces as a function of agitator
speed for comparison with calculated values using a mass transfer corre-
lation developed by J. B. Lewis.[18]

Experiment MTE-3 (shown schematically in Fig. 6) consisted of three
interconnected vessels: a 14-in.-diam fuel salt reservoir, a 10-in.-
diam salt-metal contactor, and a 6-in.-diam rare-earth stripper. The salt-
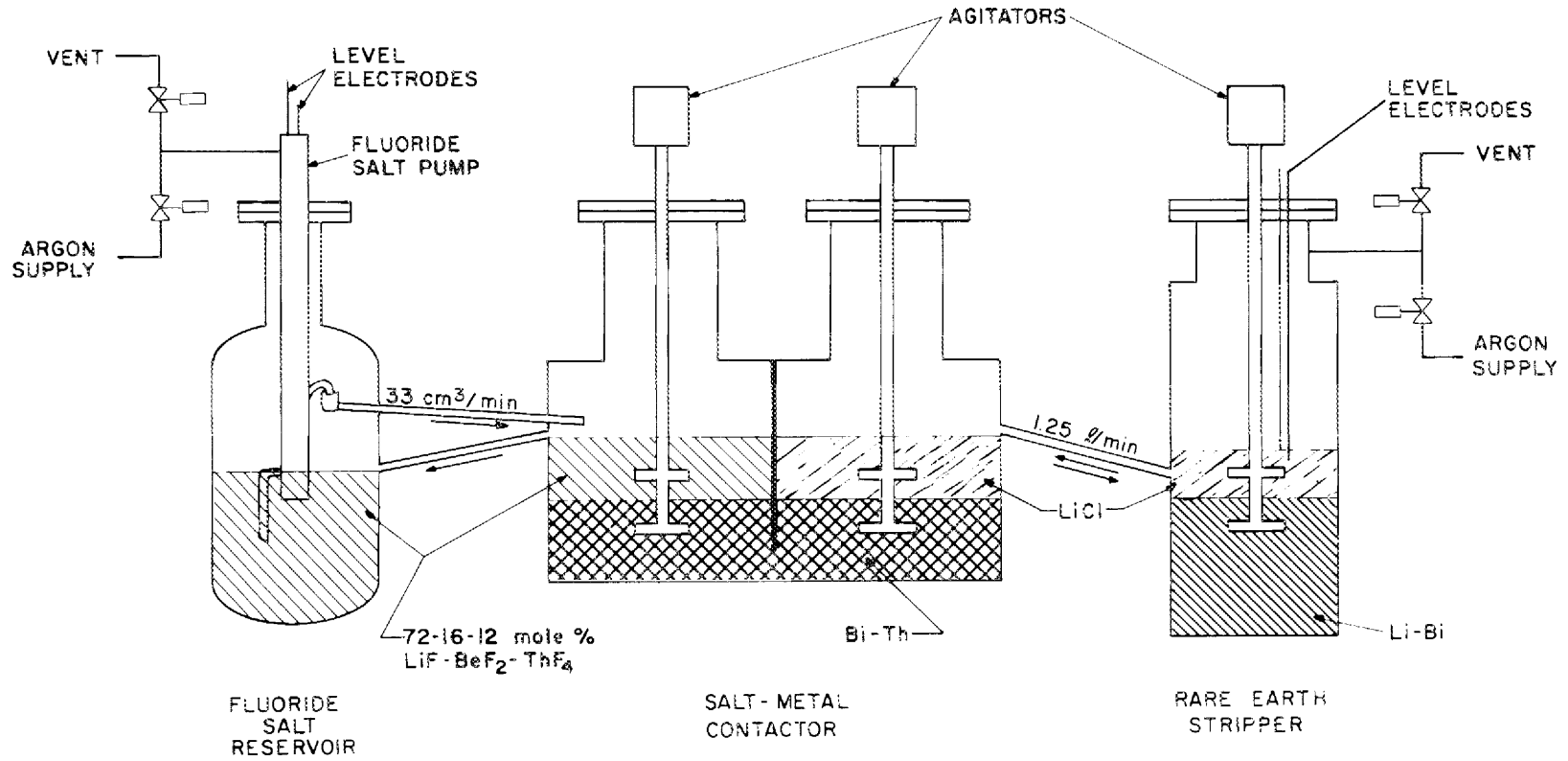metal contactor was divided into two compartments that were interconnected

Fig. 6. Flow diagram for metal transfer experiment MTE-3.

through an opening in the bottom of the divider by a pool of bismuth containing thorium and lithium. The stripper contained an Li-Bi solution. A mechanical agitator was used in each compartment of the contactor and in the Li-Bi stripper to promote mass transfer across the three salt-metal interfaces. All vessels were fabricated of carbon steel and had an oxidation-resistant coating of nickel aluminide on the outside surfaces.

The purpose of experiment MTE-3 was to evaluate the contactor and stripper described above for use in removing rare earths from molten-salt reactor fuel. Fluoride and LiCl flow rates were about 1% of those required for removing rare earths from a 1000-MW(e) MSBR. The operating temperature was about 650°C; the phases were 72-16-12 mole % LiF-BeF$_2$-ThF$_4$ fuel carrier salt, 0.13 at. % Th-Bi solution containing about 100 wt ppm of lithium as reductant, and a 5 at. % Li-Bi solution in the stripper. In this process, the rare earths are extracted from the carrier salt into the Th-Bi solution. The rare earths are extracted from the Th-Bi into molten LiCl and are subsequently stripped from the LiCl into Bi-Li alloy.

Mass transfer coefficients for radium, europium, lanthanum, and neodymium were measured during 13 runs for comparison with values predicted by literature correlation.[18] Agitator speeds of 100 to 400 rpm were used. Many of the mass transfer coefficients were found to be substantially lower (4 to 15%) than predicted.[19] Termination of the MSR Program precluded further investigation of the mass transfer rates and postoperative examination of the MTE-3 equipment to determine the reason for the lower-than-expected transfer rates. The system was shut down and placed in standby condition, with all salt and metal phases frozen, in February 1973.

We plan to continue studies of the mass transfer rates of rare earths between fuel carrier salt, bismuth, and LiCl in a new experiment designated as MTE-3B. New vessels, salts, and bismuth will be used.

3.1 Examination of MTE-3 Equipment and Materials

Metal transfer experiment MTE-3 was maintained at approximately 650°C for about 1 year (∿8700 hr). During the final run (EU-9), in which an agitator speed of 400 rpm was employed, fluoride salt was entrained into the LiCl in the contactor[17] (∿10 wt % fluoride into the LiCl). This resulted in the transfer of thorium into the LiCl, from which it was subsequently extracted into the Li-Bi solution in the stripper. After run EU-9 the experiment was shut down, cooled to room temperature, and placed in standby. (This was in February 1973 when the MSR Program was terminated.)

Removal of the three agitator assemblies for examination of the molybdenum shafts and agitator blades and, if feasible, reuse in experiment MTE-3B required that the salt and metal phases in the contactor and stripper vessels be melted. After all heater circuits and recalibration of instrumentation had been checked, the contactor and stripper vessels were heated to approximately 650°C and the agitator assemblies were removed without difficulty. The agitator ports were immediately sealed with blank flange cover plates and the vessels cooled to ambient temperature. During the removal of the agitators, an argon atmosphere was maintained in the vessels.

A cursory visual examination indicated that the molybdenum shaft and blades were in good condition. No areas of heavy corrosion attacks were noted. However, some areas of the shaft and blades contain deposits of salt and metal which must be removed for a more-detailed and meaningful examination. Therefore, whether or not the molybdenum agitator can or should be used in experiment MTE-3B has not been determined. (Note: The shaft on the agitator from the LiCl side of the contactor was accidently broken, after removal, in an attempt to remove the pin holding the molybdenum shaft to the agitator drive unit.) Figure 7 is a photograph of the molybdenum agitator shafts as removed. Note that the agitator from the LiCl side of the contactor shaft is hollow at the break point. This is not in accord with the engineering drawing for the shaft (M12172 CD 027 E Rev. 5), which indicates a solid construction at the broken areas.

27

CONTACTOR
Fluoride Salt--Bi-Th

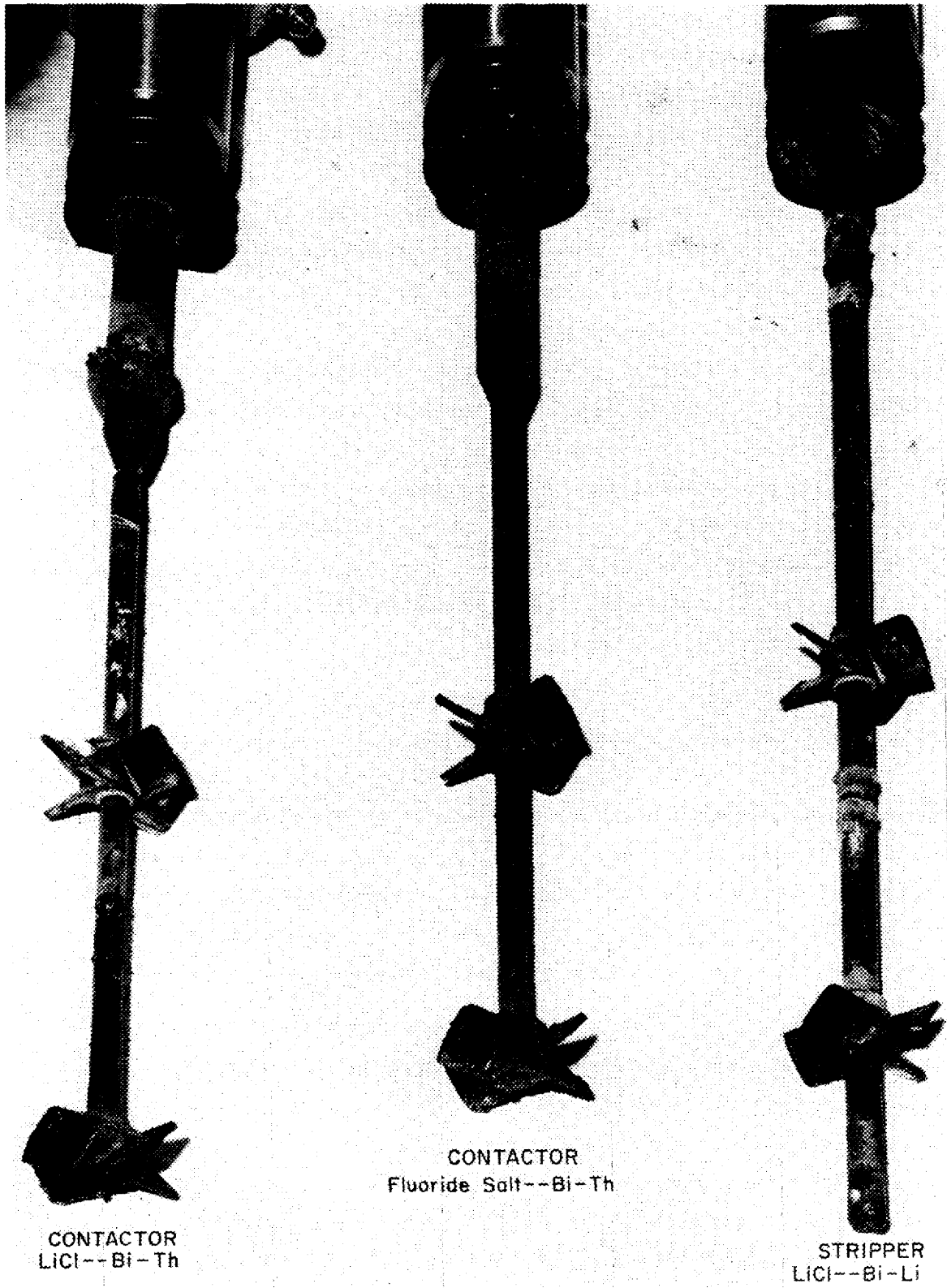CONTACTOR
LiCl--Bi-Th

STRIPPER
LiCl--Bi-Li

Fig. 7. Photograph of agitator shafts removed from MTE-3.

We removed the thermal insulation from MTE-3 and some of the stainless steel shim stock surrounding the electric heaters. The outside surfaces of the carbon steel vessels (ASTM-A106 Grade B with a nominal composition of Fe; C, 0.30% max; Mn, 0.29-1.06%; P, 0.048% max; S, 0.058% max; Si, 0.10% min) were found to be badly oxidized due to failure of the oxidation-resistant coating. These vessels had been maintained at ~650°C for approximately 1 year (~8700 hr). The depth of oxidation was estimated to be 1/16 in. or less and thus did not significantly affect the mechanical integrity of the vessels (initial wall thickness = 3/8 in.) at the operating conditions of MTE-3. The oxidation-resistant protective coating consisted of 0.015- to 0.020-in.-thick nickel aluminide[*] applied by flame spraying with wire flame spray equipment. We contacted a representative of METCO, who recommended that a much better coating would be obtained by using a nickel-chromium alloy with aluminum composite in powder form (METCO No. P443-10) applied with plasma spray equipment. Test sections of carbon steel pipe with the two coatings described above have been prepared for comparative evaluation.

We obtained samples of the salts (fuel carrier salt and LiCl) and bismuth from the MTE-3 vessels by removing a 2-in.-diam plug across each salt-metal interface. A layer of material of different structure (~1/3 in. thick) appeared to exist between the LiCl--Li-Bi phases in the stripper, whereas no comparable film was seen at the interfaces between the LiCl--Bi-Th and the fuel carrier salt--Bi-Th phases in the contactor. Corrosion of the inside surfaces of the 2-in.-diam vessel wall sections appeared minimal on visual examination of the 2-in.-diam plugs.

A small (~1/8- by ~1/4-in.) sample of bismuth was taken at each of the three metal-salt interfaces for metallographic examination. Each section included the bismuth surface in contact with the salt phase. Photomicrographs of these samples are shown in Figs. 8-10. As seen, there is some foreign material at each surface of the bismuth which was in contact with the salt phase (fluid carrier salt and LiCl). Whether this material was present during operation of metal transfer experiment

---

[*]METCO No. M405-10 (METCO, Inc., Westbury L.I., N.Y.).
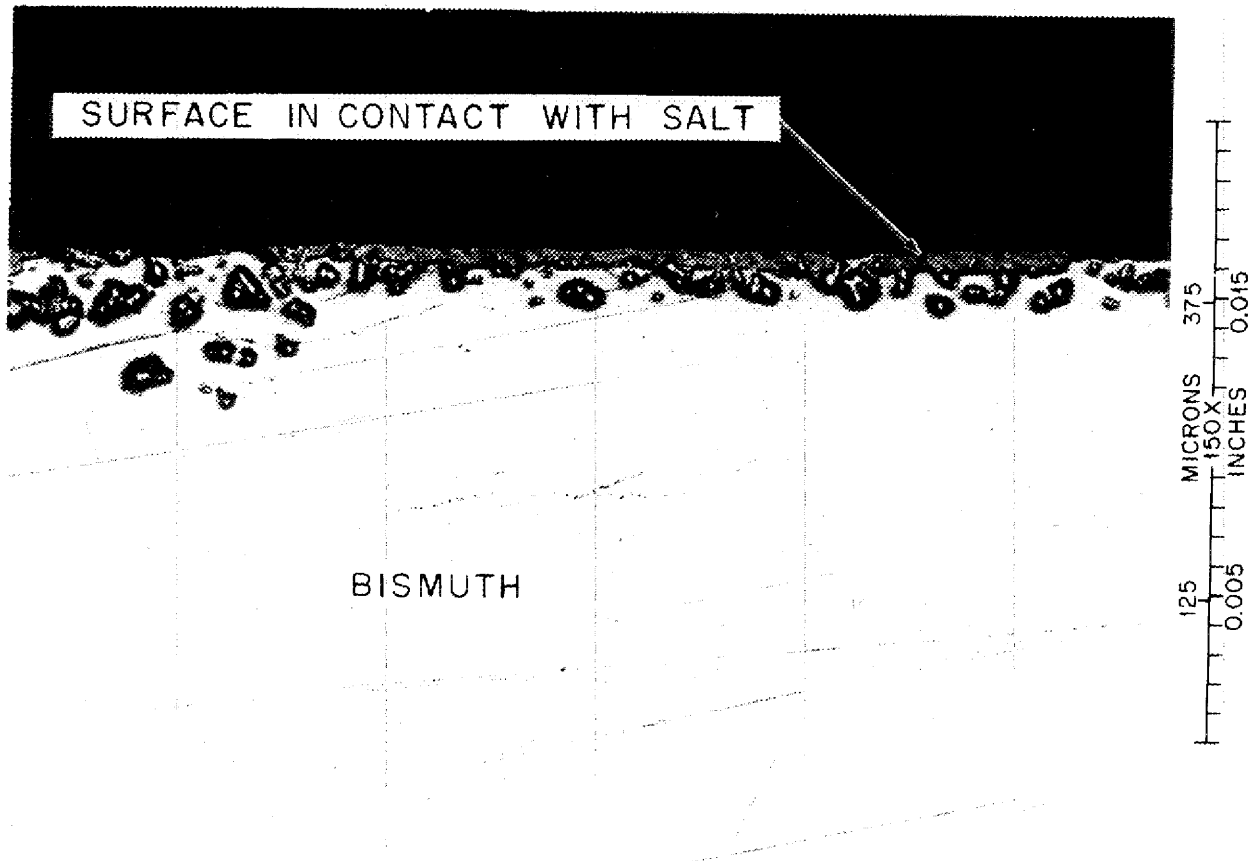
ORNL DWG. 74-10113

Fig. 8. Photomicrograph of Bi-Th phase from the contactor at the fluoride carrier salt interface in experiment MTE-3. As polished. 150X.
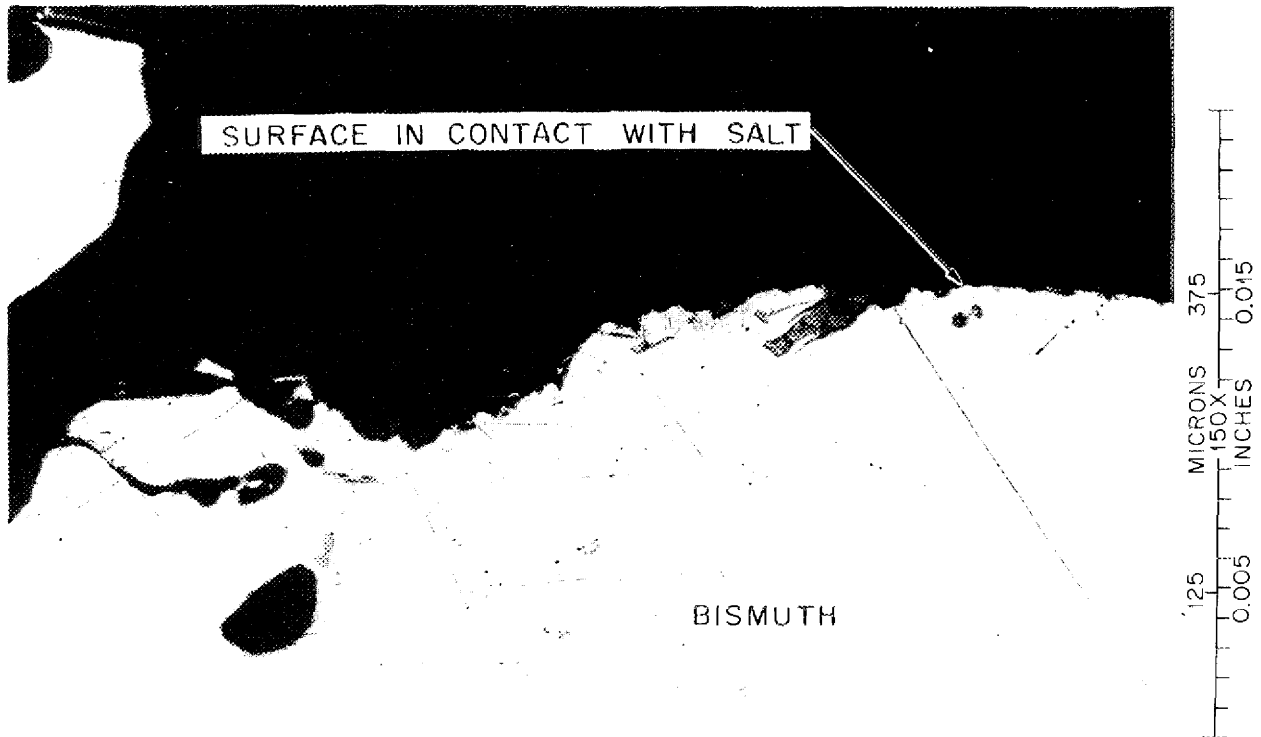
ORNL DWG. 74-10114

Fig. 9. Photomicrograph of Bi-Th phase from the contactor at the LiCl interface in experiment MTE-3. As polished. 150X.

31

Fig. 10. Photomicrograph of Li-Bi phase from the stripper vessel at the LiCl interface in experiment MTE-3. As polished. 100X.

MTE-3 or segregated at the surface when the phases were cooled without agitation is unknown.

Scanning electron microprobe analyses were performed to identify the material seen at the interfacial surfaces of the bismuth. Results are shown in Figs. 11-13. The bismuth in contact with the fluoride carrier salt contained a surface layer which was enriched with thorium and iron. Thorium and iron, along with some manganese and lanthanum (lanthanum was one of the rare earths used to measure mass transfer rates in MTE-3), were identified at the surface of the bismuth in contact with the LiCl in the contactor. Iron and thorium were also identified at the surface of the bismuth in contact with the LiCl in the stripper. The Bi-Th and the Li-Bi phases, as well as the salt phases, contained significant amounts of iron (see Table 4), undoubtedly as a result of corrosion of the carbon steel vessels. A petrographic examination was made of a sample of the fluoride salt from the contactor at a point near the Bi-Th phase and the tank wall. This examination indicated that the sample consisted principally of crystals of $3LiF-ThF_4$. According to the phase diagram of the 72-16-12 mole % $LiF-BeF_2-ThF_4$, $3LiF-ThF_4$ would be expected to crystallize from solution on cooling--especially at or near the tank wall. No oxides were found in the sample.

A section of the Li-Bi--LiCl across the interfacial area from the stripper (which included the layer of material of different structure between the Li-Bi and the LiCl) is being examined by scanning electron microscopy. No results have been obtained as yet.

3.2   Status of Experiment MTE-3B

We plan to continue measuring the mass transfer rates of rare earths between salt and bismuth in a new experiment, which is designated as MTE-3B. The vessels, salts, and bismuth that were used for MTE-3 will be discarded. New carbon steel vessels are being fabricated, with mid-June being the estimated completion date. After the vessels have been received, assembly of the equipment will begin. Based on the results of MTE-3, initial experiments will be made at agitator speeds up to 300 rpm.

Y-124404

Backscattered Electrons

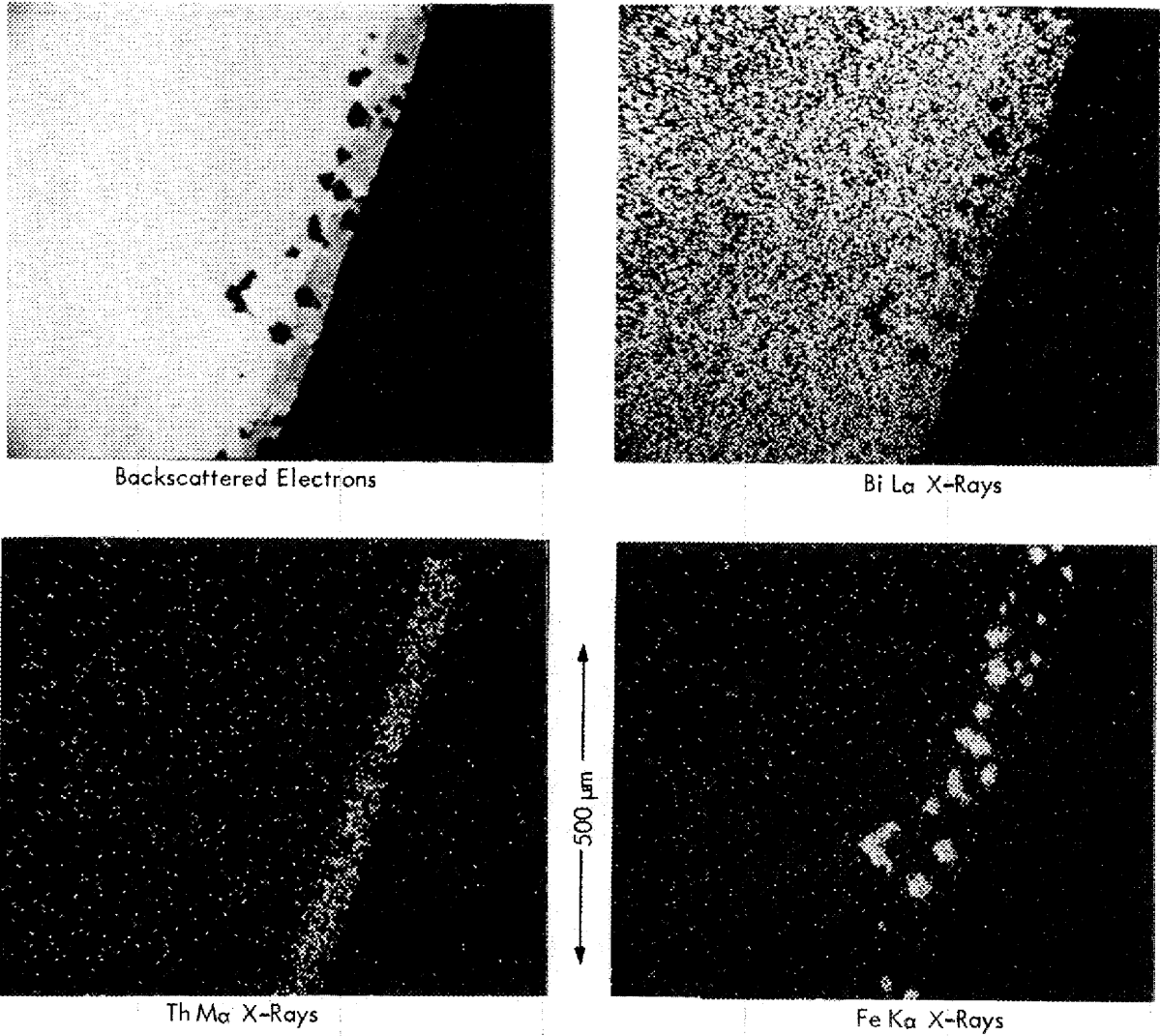Bi Lα X-Rays

500 μm

Th Mα X-Rays

Fe Kα X-Rays

Fig. 11. Electron beam scanning images of elements in the Bi-Th
phase from the contactor at the fluoride salt interface in experiment
MTE-3.

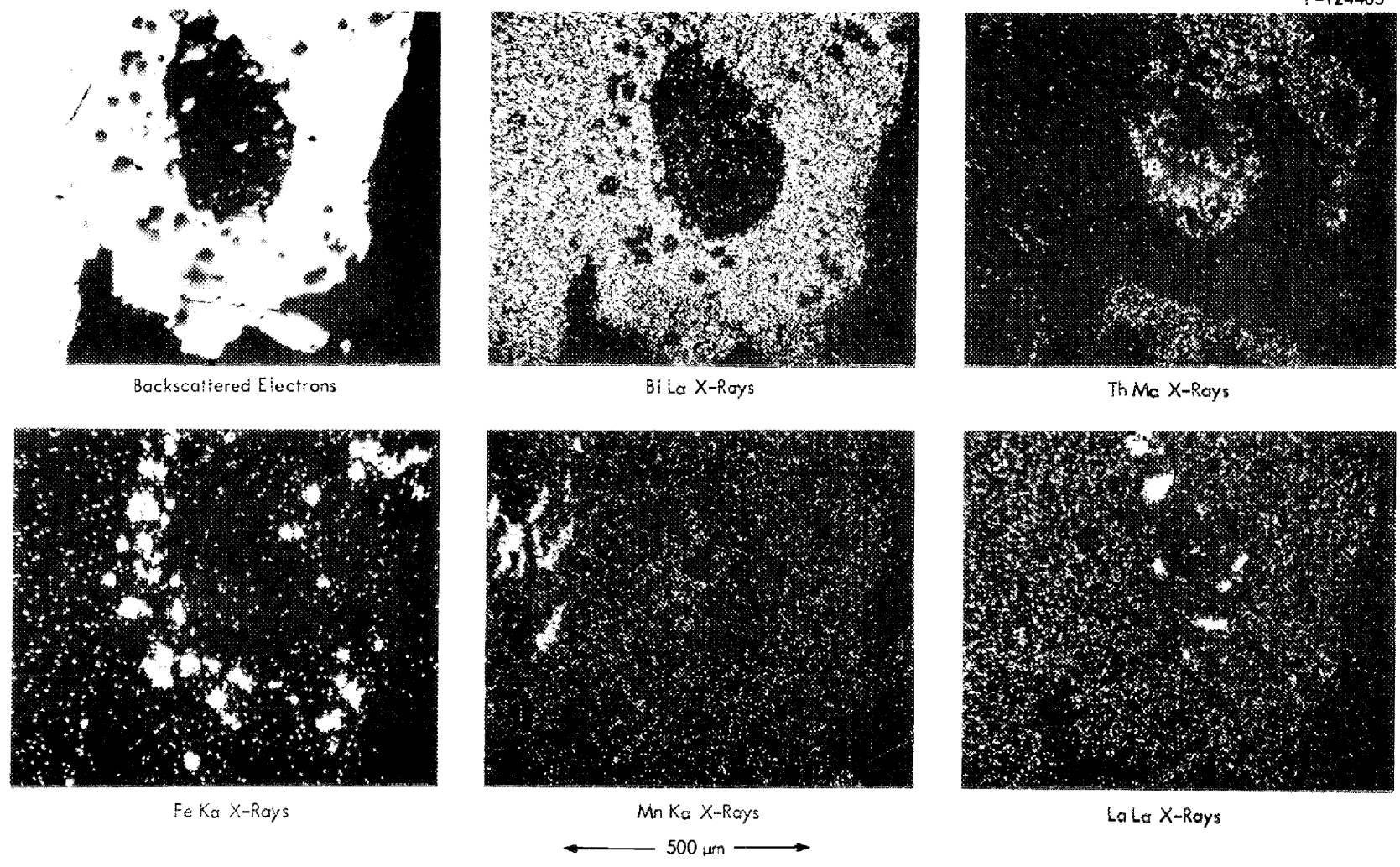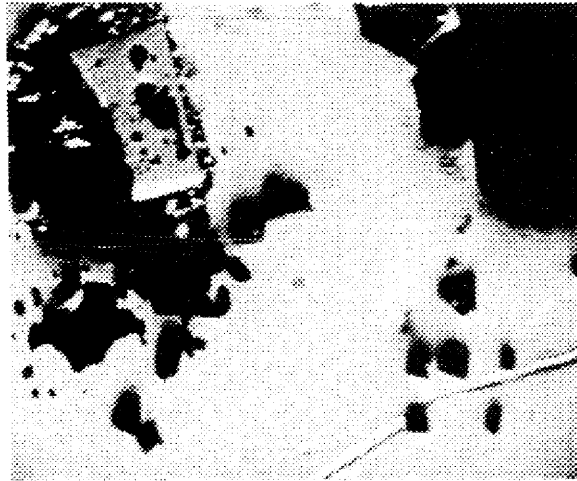Fig. 12. Electron beam scanning images of elements in the Bi-Th
phase from the contactor at the LiCl salt interface in experiment MTE-3.
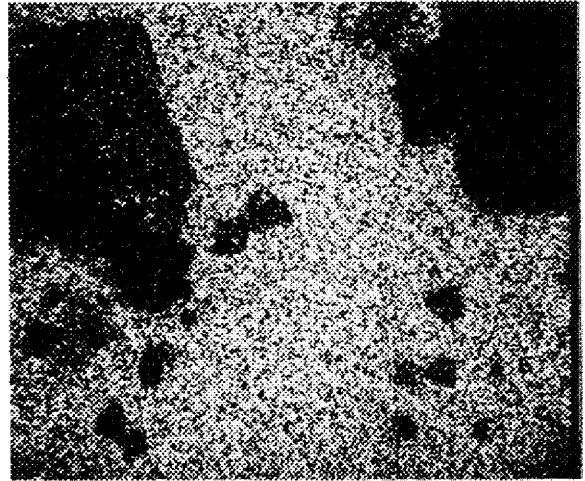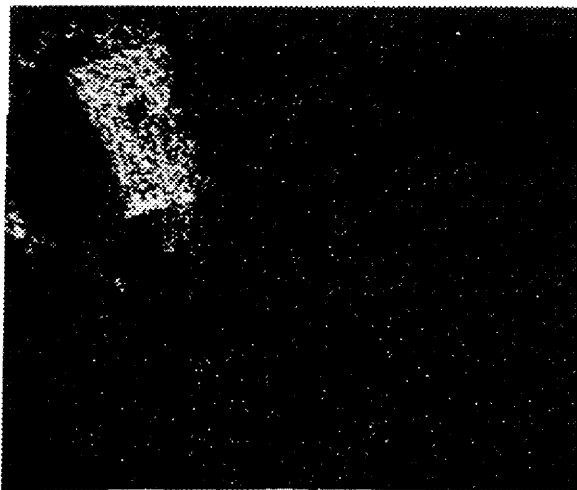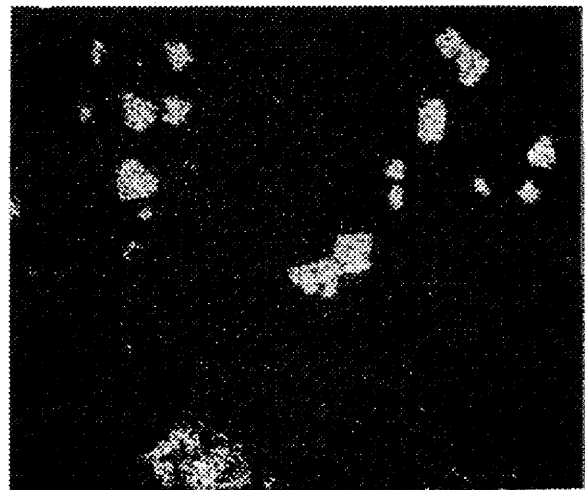
Y-124403

Fig. 13. Electron beam scanning images of elements in the Li-Bi phase from the stripper at the LiCl salt interface in experiment MTE-3.

Table 4. Iron content of samples of metal and salt phases
from metal transfer experiment MTE-3

Material	Fe (ppm)
Fluoride salt from contactor	320, 88[a]
Bi-Th, fluoride-salt side of contactor	1100
Bi-Th, LiCl side of contactor	2500
LiCl from contactor	3500
LiCl from stripper	650
Li-Bi from stripper	1400

[a]Results for two different samples. All other results are for one sample.

Earlier data showed that improved transfer rates were observed with increasing speed; however, at 400 rpm, fluoride salt was entrained into the LiCl salt.[17] We plan to use ^{147}Nd as the rare earth. As in experiment MTE-3, transfer rates can readily be followed by counting the 0.53-MeV gamma emitted by ^{147}Nd. Also, the relatively short half-life of ^{147}Nd (11 days) will allow experiments to be repeated after a reasonable waiting period.

4. CONTINUOUS FLUORINATOR DEVELOPMENT

R. M. Counce   J. R. Hightower, Jr.

4.1 Autoresistance Heating Tests

A nonradioactive experiment to demonstrate that a layer of frozen salt
will provide protection against corrosion in a continuous fluorinator
requires a heat source in the molten salt which is immune to attack by
the gaseous fluorine. We have previously shown[20] that autoresistance
heating of the salt is feasible, and have designed and built a fluorinator
mock-up to test a design for an electrode sidearm to keep the electrode
out of the fluorine stream.[21]

Five experiments (AHT-1 through -5) were run in the fluorinator mock-
up before the MSR Program was interrupted (between January 1973 and
January 1974). This equipment remained idle, but intact, during this
period. The equipment has now been returned to operating condition, and
testing of autoresistance heating in it has been resumed.

Experiments AHT3-6A, -6B, -7, -8, and -9 were carried out during this
report period. In runs AHT3-6A, -6B, -8, and -9, the autoresistance
heating was begun when the wall temperature of the test section was cooled
to 350°C, the lowest temperature at which liquid can exist in the LiF-
BeF_2-ThF_4 system. No internal heating was attempted in run AHT3-7.

The circuit resistance during cooldown in runs AHT3-6A and -6B
remained at about 0.01 to 0.03 Ω until the wall temperature dropped to
approximately 500°C, where the fuel salt begins to freeze. As the wall
temperature decreased from 500°C to 350°C, the resistance increased; at
about 350°C, it increased dramatically. Presumably, this occurred because
the salt film becomes completely nonconducting only when the temperature
is sufficiently low to preclude the existence of liquid. In the LiF-BeF_2-
ThF_4 system, no liquid can exist below 350°C.

When the wall temperature reached 350°C, autoresistance heating was
started. We had planned to increase the current through the salt until
the wall temperatures indicated steady state. However, steady state was

not attained. Instead, the resistance through the conducting path decreased suddenly from 0.5 Ω in run 6A and 0.4 Ω in run 6B to zero, indicating a loss of film integrity and subsequent shorting of the heating current.

Increases in the wall temperatures at the time of shorting indicated that the shorting occurred near the bend in the electrode sidearm nearest to the electrode. This was thought to be due to localized high current densities. The sidearm and other critical areas of the test vessel have been modeled to determine if localized high current densities might exist. The modeling procedure and results are discussed in the next section.

In run AHT3-7, the wall temperature of the test vessel was lowered to 425°C and the remaining liquid salt was transferred to the feed tank. Internal heat generation was not attempted. The frozen salt wall was inspected after the equipment had been cooled to room temperature. The salt was almost completely frozen across the vessel just above the lower sidearm inlet, although a much thinner salt layer (∿3/4 in.) was present just below the inlet and higher in the test section. This freezing was caused by contact of the unheated argon with the liquid salt. Heaters have been added on the argon lines to the test vessel to help alleviate this problem.

After the effects of the cold argon had been reduced, the maximum resistance during autoresistance heating increased dramatically in AHT3-6A and -6B to 0.5 and 0.4 Ω, respectively. In run AHT3-8, which was made after heaters had been added on the argon lines, the maximum resistance was 2.4 Ω during autoresistance heating. During the period of autoresistance heating (25 min), the current was increased from 5 A to 24 A. The salt temperatures continued to decrease during this time but appeared to be approaching a constant value (above room temperature). After 25 min of autoresistance heating, the resistance suddenly decreased while the temperature rose rapidly in the bend of the electrode sidearm near the electrode, indicating that this was the area in which the salt film had melted.

Experiment AHT3-9 was performed using the same procedure as before, except that the current was limited to a maximum of 17 A. The electrode

in these tests consisted of a 1/2-in. Inconel tube extending to the inter-
section of the centerlines of the vertical section and the sloping section
of the electrode sidearm (see ref. 21). In the first nine runs, the salt
depth in the electrode sidearm above the end of the tube was measured by
bubbling argon through the tube. Before run AHT3-9 was started, this
measurement had indicated that the salt level in the sidearm was lower
than that measured in the main compartment (gas-salt contacting zone) of
the test vessel. Also, abnormally high resistances were observed during
this run. The highest resistance during autoresistance heating in AHT3-9
was 4.3 Ω. At the end of the experiment, the salt was transferred to the
feed tank from the test vessel. The captive volume of salt in the elec-
trode sidearm could not be removed. After the equipment had been allowed
to cool, the electrode was removed and examined. The lower 6 in. of the
1/2-in. Inconel tube of which the electrode was made was missing. Thus
far, we have no explanation for this phenomenon.

4.2 Distribution of Current Densities in the
Autoresistance Heating Equipment

We have constructed an electrical analog of the electrode sidearm in
order to determine if there are regions of localized high current density
which might be causing the frozen salt film near the electrode to melt.
The analog was made from electrically conducting photographic paper[*] cut
in the shape of the sidearm and the contained electrode. With the use of
this special paper, a two-dimensional model may be constructed for the
study of steady-state current flow in simple or complex geometry.[22]

The geometric model used isopotential nonconducting wall conditions,
which were represented in the model by lines of conductive paint.[**] By
giving the opposing walls separate and distinct potentials, we were able
to produce an electric field which could be mapped using a high-impedance
voltmeter with an electric probe.

---

[*]Grade 506-L, distributed by Knowlton Bros., Watertown, N. Y. The resis-
tance of this paper was sufficiently high for use in this study.
[**]Silver paint obtained from Dupont Electrochemicals, Wilmington, Del.

The isopotential lines generated between the walls in this manner represented current flow lines. By shifting the electrodes 90° to the ends of the model, the isopotentials would represent the potential gradient in the system.

The Bivar potential source and probe used for measuring the electric field were made by Electronic Associates, Inc., of Long Beach, New Jersey. An accompanying Variplotter, also made by Electronic Associates, Inc., provided the connections to the voltage source and an insulated surface to hold the model. A high-impedance voltmeter was required to measure the field potentials.

The lines in Figs. 14-16 represent current stream lines. The distance between two stream lines in Fig. 14 represents the passage of 12.5% of the total current. In Figs. 15 and 16, the distance between stream lines represents 10% of the total current.

Figures 14 and 15 show that there are no regions of abnormally high current densities in the vicinity of the two bends in the electrode sidearm. The present sidearm design seems adequate with regard to localized heat generation rates.

Figure 16 shows an alternate electrode design which would further reduce localized heating at the sidearm bend near the electrode. This design has the additional advantage that it could also be used as the device for introducing the feed to the fluorinator without fear of impinging a jet of hot salt against the frozen wall and destroying the insulating film near the electrode.
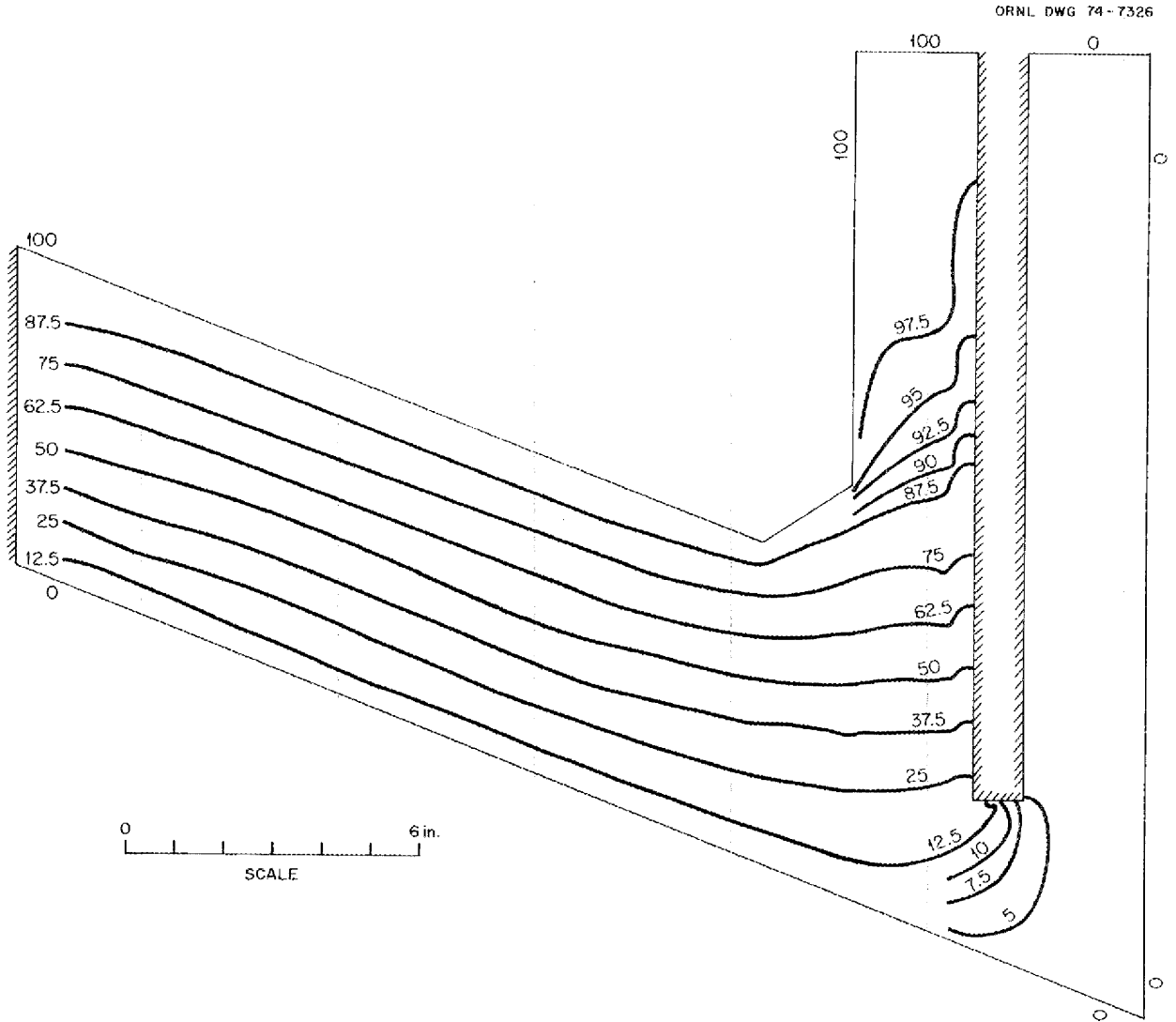
Fig. 14. Calculated current distribution in the electrode sidearm of autoresistance heating test AHT-3. The percentage of the total current flowing between two stream lines is equal to the difference between the numbers on the stream lines.
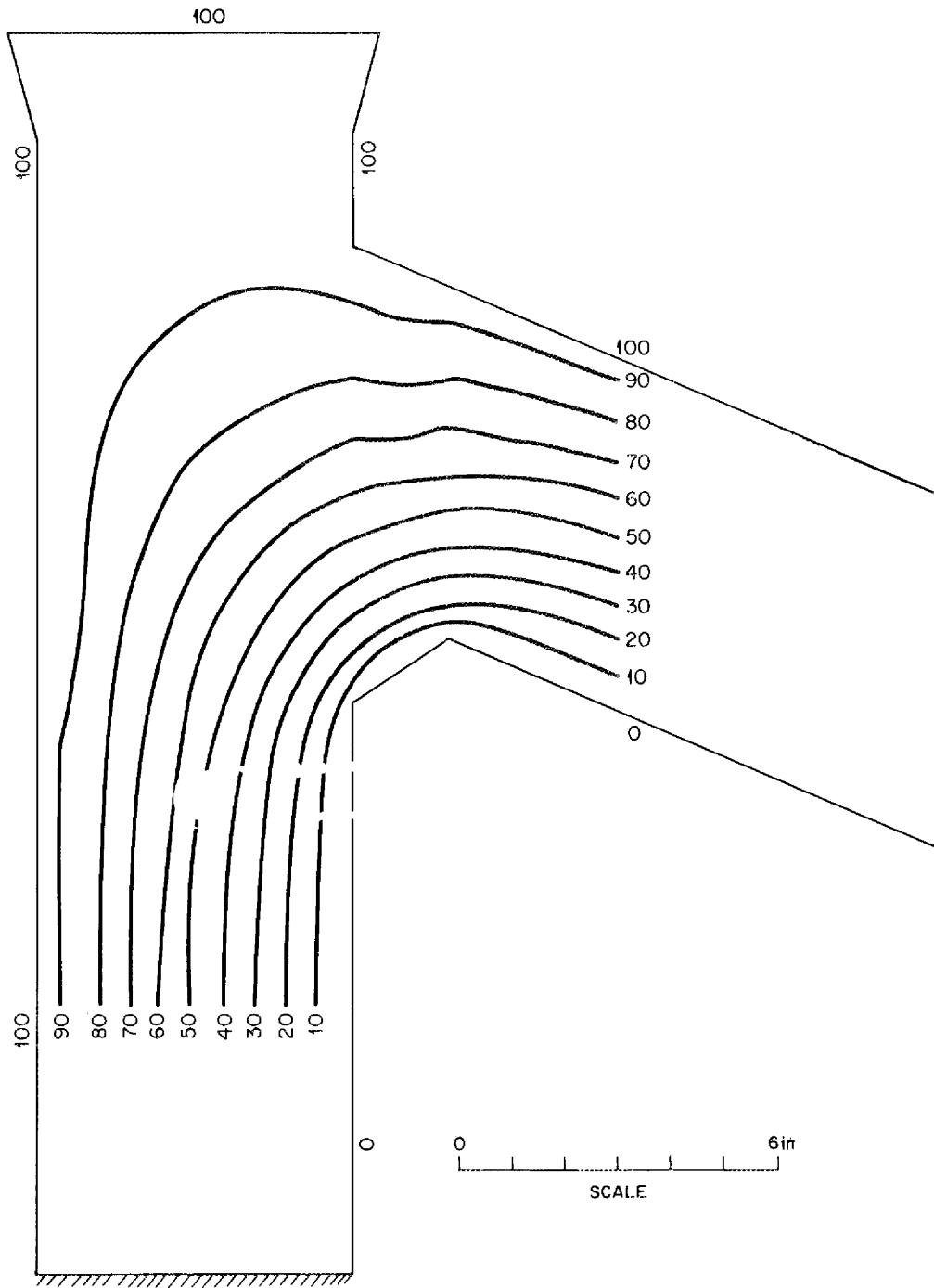
Fig. 15. Calculated current distribution at the junction of the electrode sidearm and the fluorination section in autoresistance heating test AHT-3. The percentage of total current flowing between two stream lines is equal to the difference between the numbers on the stream lines.
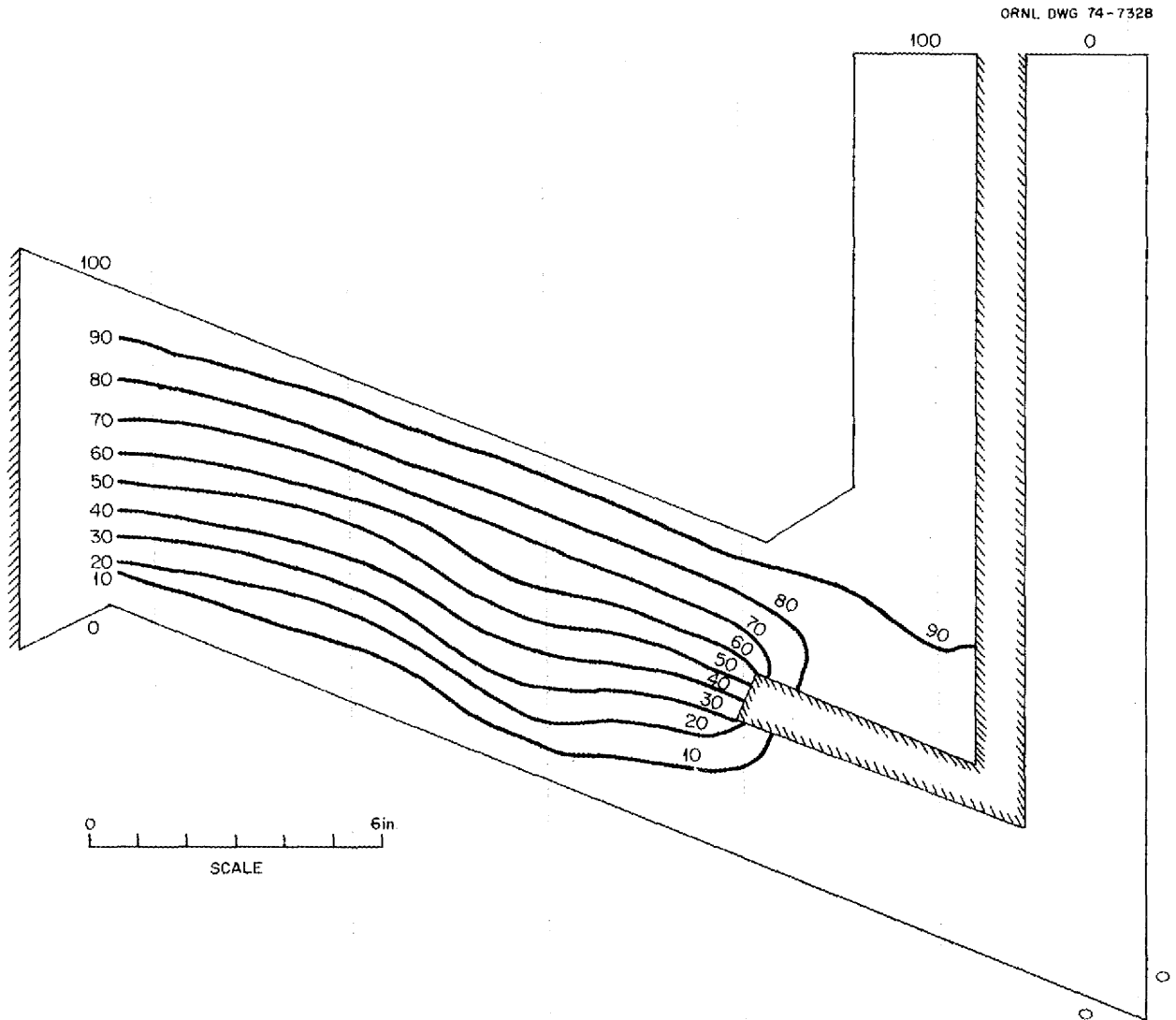
ORNL DWG 74-7328

Fig. 16. Calculated current distribution in the electrode sidearm using a new electrode design. The percentage of the total current flowing between two stream lines is equal to the difference between the numbers on the stream lines.

5. REFERENCES

1. J. B. Lewis, Chem. Eng. Sci. 3, 248-59 (1954).

2. W. J. McManamey, Chem. Eng. Sci. 18, 123-32 (1961).

3. G. R. A. Mayers, Chem. Eng. Sci. 16, 69-75 (1961).

4. J. A. Klein, in Engineering Development Studies for Molten-Salt Breeder Reactor Processing No. 14, ORNL-TM-4018 (in preparation).

5. J. A. Klein, in Engineering Development Studies for Molten-Salt Breeder Reactor Processing No. 15, ORNL-TM-4019 (in preparation).

6. Chem. Technol. Div. Annu. Progr. Rept. Mar. 31, 1973, ORNL-4883, pp. 23-25.

7. B. A. Hannaford, C. W. Kee, and L. E. McNeese, MSR Program Semiannu. Progr. Rept. Feb. 28, 1971, ORNL-4676, p. 256.

8. B. A. Hannaford et al., MSR Program Semiannu. Progr. Rept. Aug. 31, 1971, ORNL-4728, p. 212.

9. B. A. Hannaford, C. W. Kee, and L. E. McNeese, Engineering Development Studies for Molten-Salt Breeder Reactor Processing No. 8, ORNL-TM-3259, p. 64.

10. B. A. Hannaford, C. W. Kee, and L. E. McNeese, Engineering Development Studies for Molten-Salt Breeder Reactor Processing No. 9, ORNL-TM-3259, p. 158.

11. B. A. Hannaford, C. W. Kee, and L. E. McNeese, Engineering Development Studies for Molten-Salt Breeder Reactor Processing No. 10, ORNL-TM-3352, pp. 12-20.

12. A. S. Foust et al., Principles of Unit Operations, p. 210, Wiley, New York, 1960.

13. MSR Program Semiannu. Progr. Rept. Aug. 31, 1971, ORNL-4728, pp. 179-83.

14. L. E. McNeese, Engineering Development Studies for Molten-Salt Breeder Reactor Processing No. 7, ORNL-TM-3257, pp. 29-46.

15. L. E. McNeese, Engineering Development Studies for Molten-Salt Breeder Reactor Processing No. 9, ORNL-TM-3259, pp. 167-94.

16. L. E. McNeese, Engineering Development Studies for Molten-Salt Breeder Reactor Processing No. 11, ORNL-TM-3774 (in preparation).

17. L. E. McNeese, _Engineering Development Studies for Molten-Salt Breeder Reactor Processing No. 17_, ORNL-TM-4178 (in preparation).

18. J. B. Lewis, Chem. Eng. Sci. _3_, 248-59 (1954).

19. _Chem. Technol. Div. Annu. Progr. Rept. Mar. 31, 1973_, ORNL-4883, p. 25.

20. J. R. Hightower, Jr., _Engineering Development Studies for Molten-Salt Breeder Reactor Processing No. 16_, ORNL-TM-4020 (in preparation).

21. J. R. Hightower, Jr., _Engineering Development Studies for Molten-Salt Breeder Reactor Processing No. 17_, ORNL-TM-4178 (in preparation).

22. C. F. Kayan, "An Electric Geometrical Analogue for Complex Heat Flow," Trans. ASME _67_(8), 713-16 (1945).

ORNL-TM-4698
UC-76 — Molten Salt Reactor Technology

INTERNAL DISTRIBUTION

1-2. MSRP Director's Office	62. B. F. Hitch
3. C. F. Baes, Jr.	63. R. W. Horton
4. C. E. Bamberger	64. W. R. Huntley
5. M. Bender	65. C. W. Kee
6. M. R. Bennett	66. A. D. Kelmers
7. E. S. Bettis	67. J. A. Klein
8. R. E. Blanco	68. W. R. Laing
9. J. O. Blomeke	69. R. B. Lindauer
10. E. G. Bohlmann	70. R. E. MacPherson
11. J. Braunstein	71. W. C. McClain
12. M. A. Bredig	72. H. E. McCoy
13. R. B. Briggs	73. A. P. Malinauskas
14. H. R. Bronstein	74. C. L. Matthews, AEC-OSR
15. R. E. Brooksbank	75. A. S. Meyer
16. C. H. Brown, Jr.	76. R. L. Moore
17. K. B. Brown	77. J. P. Nichols
18. J. Brynestad	78. K. J. Notz
19. S. Cantor	79. H. Postma
20. D. W. Cardwell	80. M. W. Rosenthal
21. W. L. Carter	81. A. D. Ryon
22. W. H. Cook	82. H. C. Savage
23. R. M. Counce	83. W. F. Schaffer, Jr.
24. J. L. Crowley	84. C. D. Scott
25. F. L. Culler	85. M. J. Skinner
26. J. M. Dale	86. F. J. Smith
27. F. L. Daley	87. G. P. Smith
28. J. H. DeVan	88. I. Spiewak
29. J. R. DiStefano	89. O. K. Tallent
30. W. P. Eatherly	90. L. M. Toth
31. R. L. Egli, AEC-OSR	91. D. B. Trauger
32. J. R. Engel	92. W. E. Unger
33. G. G. Fee	93. J. R. Weir
34. D. E. Ferguson	94. M. K. Wilkinson
35. L. M. Ferris	95. R. G. Wymer
36. L. O. Gilpatrick	96-97. Central Research Library
37. J. C. Griess	98. Document Reference Section
38. W. R. Grimes	99-101. Laboratory Records
39. R. H. Guymon	102. Laboratory Records (LRD-RD)
40-61. J. R. Hightower, Jr.	

CONSULTANTS AND SUBCONTRACTORS

103. J. C. Frye
104. C. H. Ice
105. J. J. Katz
106. E. A. Mason
107. Ken Davis
108. R. B. Richards

EXTERNAL DISTRIBUTION

109. Research and Technical Support Division, ERDA, Oak Ridge Operations Office, P. O. Box E, Oak Ridge, Tenn. 37830
110. Director, Reactor Division, ERDA, Oak Ridge Operations Office, P. O. Box E, Oak Ridge, Tenn. 37830
111-112. Director, ERDA Division of Reactor Research and Development, Washington, D. C. 20545
113-216. For distribution as shown in TID-4500 under UC-76, Molten Salt Reactor Technology